AD-A130 115 MAGNETOHYDRODYNAMIC MODELLING OF INTERPLANETARY DISTURBANCES BETWEEN THE SUN AND EARTH(U) AIR FORCE GEOPHYSICS LAB HANSCOM AFB MA M DRYER ET AL. 21 DEC 82 1/1

UNCLASSIFIED AFGL-TR-82-0396 F/G 4/1 NL

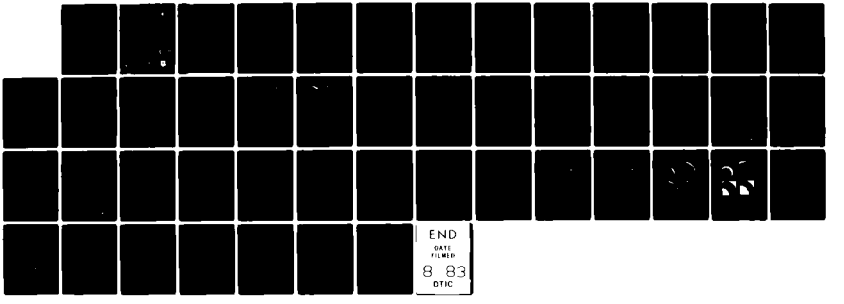

END
DATE FILMED
8 83
DTIC

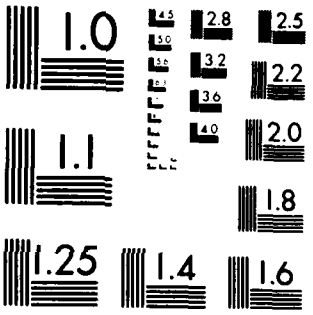

AFGL-TR-82-0396
ENVIRONMENTAL RESEARCH PAPERS, NO. 816

(12)

Magnetohydrodynamic Modelling of Interplanetary Disturbances Between the Sun and Earth

M. DRYER
S.T. WU

21 December 1982

SPACE PHYSICS DIVISION PROJECT 4643
AIR FORCE GEOPHYSICS LABORATORY
HANSCOM AFB, MASSACHUSETTS 01731

AIR FORCE SYSTEMS COMMAND, USAF

This report has been reviewed by the ESD Public Affairs Office (PA) and is releasable to the National Technical Information Service (NTIS).

This technical report has been reviewed and is approved for publication.

Alva T Stair, Jr.

DR. ALVA T. STAIR, Jr
Chief Scientist

Qualified requestors may obtain additional copies from the Defense Technical Information Center. All others should apply to the National Technical Information Service.

Unclassified

SECURITY CLASSIFICATION OF THIS PAGE (When Data Entered)

REPORT DOCUMENTATION PAGE	READ INSTRUCTIONS BEFORE COMPLETING FORM
1. REPORT NUMBER: AFGL-TR-82-0396	2. GOVT ACCESSION NO.: AD-A130115
3. RECIPIENT'S CATALOG NUMBER	
4. TITLE (and Subtitle): MAGNETOHYDRODYNAMIC MODELLING OF INTERPLANETARY DISTURBANCES BETWEEN THE SUN AND EARTH	5. TYPE OF REPORT & PERIOD COVERED: Scientific. Interim.
	6. PERFORMING ORG. REPORT NUMBER: ERP, No. 816
7. AUTHOR(s): M. Dryer*, S. T. Wu**	8. CONTRACT OR GRANT NUMBER(s)
9. PERFORMING ORGANIZATION NAME AND ADDRESS: Air Force Geophysics Laboratory (PHY), Hanscom AFB, Massachusetts 01731	10. PROGRAM ELEMENT, PROJECT, TASK AREA & WORK UNIT NUMBERS: 46430801, 62101F
11. CONTROLLING OFFICE NAME AND ADDRESS: Air Force Geophysics Laboratory (PHY), Hanscom AFB, Massachusetts 01731	12. REPORT DATE: 21 December 1982
	13. NUMBER OF PAGES: 48
14. MONITORING AGENCY NAME & ADDRESS(if different from Controlling Office)	15. SECURITY CLASS. (of this report): Unclassified
	15a. DECLASSIFICATION DOWNGRADING SCHEDULE

16. DISTRIBUTION STATEMENT (of this Report)

Approved for public release; distribution unlimited.

17. DISTRIBUTION STATEMENT (of the abstract entered in Block 20, if different from Report)

18. SUPPLEMENTARY NOTES *Space Environment Laboratory.
**University of Alabama at Huntsville. Work was conducted by Space Environment Laboratory, National Oceanic and Atmospheric Administration, Boulder, Colorado 80303, under Project Order No. 2-0944.
Project Officer: Mr. Jurgen Buchau (PHY)

19. KEY WORDS (Continue on reverse side if necessary and identify by block number)

MHD modelling
Solar wind
Interplanetary disturbance

20. ABSTRACT (Continue on reverse side if necessary and identify by block number)

A time-dependent, nonplanar, two-dimensional (2-D) magnetohydrodynamic computer simulation model is used to simulate a series of solar flare-generated shock waves and their subsequent disturbances in interplanetary space between the sun and the earth's magnetosphere. The "canonical" or anzatz series of shock waves include initial velocities near the sun over the range 500 to 3000 km sec^{-1}. The ambient solar wind, through which the shocks propagate, is taken to be a steady-state flow that is independent of heliolongitude; its radial dependency consists of a representative set of plasma and magnetic field

DD FORM 1 JAN 73 1473 EDITION OF 1 NOV 65 IS OBSOLETE

Unclassified

SECURITY CLASSIFICATION OF THIS PAGE (When Data Entered)

20. Abstract (Contd)

parameters which will be presented.

Particular attention is directed to the MHD model's ability to address fundamental operational questions regarding the long-range forecasting of geomagnetic disturbances. These questions are: (1) will a disturbance (such as the present canonical series of solar flare shock waves) produce a magnetospheric and ionospheric disturbance, and, if so; (2) when will it start; (3) how severe will it be; and (4) how long will it last? The model's output is used to compute various solar wind indices of current interest for this purpose.

It is concluded that future work should be focused on a cohesive updating of, for example, daily measured solar parameters as input for the model whose output should be compared with spacecraft data for specific events.

Preface

One of the authors (M. Dryer) wishes to thank the Over-the-Horizon Backscatter Radar System Program Office of the Electronic Systems Division and the Air Force Geophysics Laboratory for its support via Project Order No. 2-0944. S.T. Wu wishes to acknowledge support via this Project Order and NOAA Contract Number NA82RAC-00136. We also wish to express our appreciation to Dr. Y. Kamide for reading the manuscript.

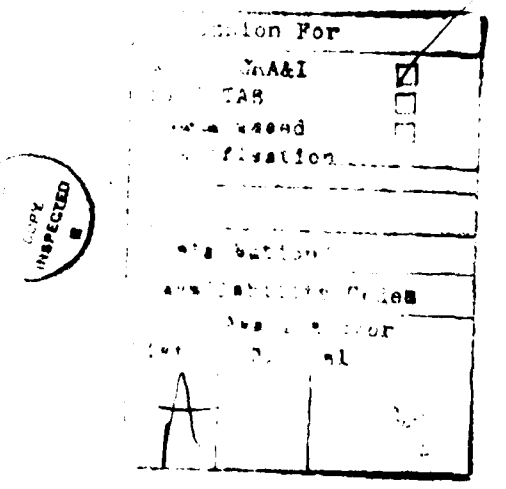

Contents

1. INTRODUCTION 7

2. ANALYSIS 10

3. GENERAL RESULTS 13

4. GEOPHYSICALLY-RELEVANT SOLAR WIND PARAMETERS 19

5. CONCLUDING REMARKS 23

REFERENCES 25

APPENDIX A: GENERAL EQUATION FOR THE CONSERVATION OF FUNDAMENTAL PHYSICAL QUANTITIES 29

APPENDIX B: ADDITIONAL RESULTS 33

Illustrations

1a. Illustration of the Spherical Coordinate System and Heliospheric Space 11

1b. Schematic Presentation of the Computational Domain, Flare Location at $\phi = 30^{o}$ (Note that $\phi = 0^{o}$ at j = 1), and Positions of Hypothetical Spacecraft Monitors 11

Illustrations

2. Total Pressure ($2nkT + B^2/8\pi$) Contours, Together with Superposition of Deformed IMF (at $t > 0$ hr), Following Introduction of the Shock Wave, $V_s = 3000$ km sec^{-1}, $\Delta t = 5400$ sec — 15

3. Three-dimensional, Polar, View of the Solar Wind Velocity Surface Within the Quadrant $0 \leq \phi \leq 90^o$ — 16

4. Time Series of Radial Solar Wind Velocity, Density, Temperature, and Total IMF Magnitude at 1.0 AU — 18

5. Shock Transit Time to 1.0 AU — 20

6. Energy Flux Parameter, ϵ, and the Product VB_θ at 1 AU for the Case $V_s = 3000$ km sec^{-1}, $\Delta t = 5400$ sec — 22

B1. Interplanetary Magnetic Field Line Deformation Following Introduction of a Solar Flare-generated Shock Wave, $V_s = 3000$ km sec^{-1} and $\Delta t = 5400$ sec — 34

B2. Temperature Contours, Together With Superposition of Deformed IMF (at $t > 0$ hr), Following Introduction of the Shock Wave, $V_s = 3000$ km sec^{-1}, $\Delta t = 5400$ sec — 35

B3. Density Contours, Together With Superposition of Deformed IMF (at $t > 0$ hr), Following Introduction of the Shock Wave, $V_s = 3000$ km sec^{-1}, $\Delta t = 5400$ sec — 37

B4. Plasma Beta ($\beta = 16\pi\, nkT/B^2$) Contours, Together With Superposition of Deformed IMF (at $t > 0$ hr), Following Introduction of the Shock Wave, $V_s = 3000$ km sec^{-1}, $\Delta t = 5400$ sec — 38

B5. Fractional Temperature Change, $(T - T_o)/T_o$, Within Part ($0 \leq \phi \leq 90^o$) of the Calculational Domain — 39

B6. Fractional Density Change, $(n - n_o)/n_o$, Within Part ($0 \leq \phi \leq 90^o$) of the Computational Domain — 40

B7. Fractional Total Pressure Change, $(P_T - P_{T_o})/P_{T_o}$ Within Part ($0 \leq \phi \leq 90^o$) of the Computational Domain — 42

B8. Time Series of Radial Solar Wind Velocity, Density, Temperature, and Total IMF Magnitude at 0.3 AU — 43

B9. Energy Flux Parameter, ϵ, and the Product VB_θ at 1 AU For the Case: $V_s = 3000$ km sec^{-1}, $\Delta t = 5400$ sec, $B_{\theta_o} = 10$ nT (Instead of 1 nT, as Used Earlier) — 46

B10. Polar Plots of IMF at 1 AU, CM, for the Case: $V_s = 3000$ km sec^{-1}, $\Delta t = 5400$ sec, $B_{\theta_o} = 10$ nT — 47

Table

1. Initial Steady-state Solar Wind Conditions — 12

Magnetohydrodynamic Modelling of Interplanetary Disturbances Between the Sun and Earth

I. INTRODUCTION

The roles of solar flares and stream-stream interactions and their effects upon the solar wind and interplanetary magnetic field (IMF) are now generally appreciated within both the scientific community and the larger group of diverse operational users of sophisticated high-technology systems. The latter group is especially concerned with magnetospheric and ionospheric disturbances during geomagnetic storms. Thus, the need for long-range forecasting (on a time scale of many hours or even several days) has become clear. An MHD model, together with several operational spacecrafts that can provide continuous "ground truth" in the solar wind, is an obvious candidate for a key role in providing this need.

This paper's purpose is to demonstrate the capability, unique at this time to our knowledge, of a self-consistent MHD model to produce operational forecasts that are specifically directed to the following questions:

(1) Will a solar disturbance affect the geophysical environment (specifically ionospheric and magnetospheric disturbances)? ... and, if so,

(2) When will a geomagnetic storm start?

(3) How long will it last?

(4) How severe will it be?

(Received for publication 9 December 1982)

It is emphasized that the MHD model that will be discussed is a development in the long tradition of simulations of initial-boundary value problems that are solved with numerical finite difference solutions of partial differential equations. The model is not a kinematical approximation as performed, for example, by Hakamada and Akasofu[1] for the kind of heliospheric problem addressed here. More specifically, we will use the model devised by Wu, Dryer, and Han.[2] This non-planar model (so-called because it includes all three components of the solar wind plasma and IMF) is the most recent development that follows upon the earlier work of Wu, Han, and Dryer;[3] Dryer, Wu, and Han;[4] D'Uston et al;[5] and D'Uston.[6] The earlier work clearly demonstrated the development of fast-forward (as well as reverse) MHD shock waves, their asymmetrical propagation, as well as their multiple interactions (as in the well-known, multiple-flare situation in August 1972). It was, however, restricted to only two components of the plasma bulk velocity and IMF in the ecliptic plane as a consequence of its purely 2-D formulation. As part of our long-range program (that includes a fully 3-D, time-dependent formulation), a non-planar extension to the earlier 2-D studies was incorporated (Wu, Dryer, and Han).[1] This "quasi-3D" or "2-1/2D" formulation now makes it possible to relate solar disturbances to geomagnetic disturbances via the studies reviewed, for example, by Smart, Garrett, and Shea.[7] We have in mind, more specifically, the use of solar wind parameters as proposed by: (1) Perreault and Akasofu[8] who advocate the use of the energy coupling function,

1. Hakamada, K., and Akasofu, S.-I. (1982) Simulation of three-dimensional solar wind disturbances and resulting geomagnetic storms, Space Sci. Rev. 31:3-70.
2. Wu, S.T., Dryer, M., and Han, S.M. (1982) Non-planar MHD model for solar flare-generated disturbances in the heliospheric equatorial plane, submitted to Solar Physics.
3. Wu, S.T., Han, S.M., and Dryer, M. (1979) Two-dimensional, time-dependent MHD description of interplanetary disturbances: simulation of high speed solar wind interactions, Planet. Space Sci. 27:255-264.
4. Dryer, M., Wu, S.T., and Han, S.M. (1980) Two-dimensional, time-dependent MHD simulation of the disturbed solar wind due to representative flare-generated and coronal hole-generated disturbances, Geofis. Intern. 19:1-15.
5. D'Uston, C., Dryer, M., Han, S.M., and Wu, S.T. (1981) Spatial structure of flare-associated perturbations in the solar wind simulated by a two-dimensional numerical MHD model, J. Geophys. Res. 86:525-534.
6. D'Uston, C. (1981) Dynamique des Ondes de Choc Interplanetaires Engendrees par des Eruptions Solaires, PhD thesis in Physical Sciences, University Paul Sabatier de Toulouse, Toulouse, France.
7. Smart, D.F., Garrett, H.B., and Shea, M.A. (1980) The prediction of AE, ap, and Dst at time lags between 0 and 30 hours, in Solar-Terrestrial Predictions Proceedings, Vol. II, R.F. Donnelly, Ed., U.S. Government Printing Office, Washington, D.C., pp. 399-413.
8. Perreault, P., and Akasofu, S.-I. (1978) A study of geomagnetic storms, Geophys. J. R. Astr. Soc. 54:547.

ϵ; and (2) Burton, McPherron, and Russell[9] who advocate the half-wave rectifier concept for the magnetosphere as represented by the quantity VB_s [*where* B_s is the southward (negative) IMF component ... corresponding, later, to our positive component, B_θ]. Other workers have examined the statistical use of these (and other) quantities for the prediction of geophysical parameters such as the AE, Dst, AL, and Kp indices (see, for example, Smart, Garrett, and Shea;[7] Baker et al;[10] Clauer et al;[11] Holzer and Slavin;[12] Kamide;[13] and Kamide and Akasofu[14]).

There is no useful purpose served if the present paper were to advocate one index in relation to another. We view our role as one that will provide all of the parameters that are used to compute the cited indices once we are provided with knowledgeable (even educated guesses!) conditions near the sun on a regular basis. [This latter phrase really means a time scale that is dependent on solar activity.] The former phrase refers to solar observations that can delineate not only solar flares (radio sweep frequency, soft X-ray), but also those that can infer the slower changes such as coronal hole (optical, magnetograph) development or demise. Only time-dependent modelling has the capability for fulfilling this requirement. Also, strictly speaking, a 3-D, time-dependent MHD model is necessary when it is known that large latitudinal changes (compared to those in the heliospheric equatorial plane) take place. We will consider this problem in the future. Stated mathematically, our present quasi-3D model will, then, assume that partial derivatives of all dependent variables (density, temperature, velocity, IMF) with respect to the heliocolatitude, θ, are negligible in comparison with those derivatives in the radial (r) and heliolongitudinal (ϕ) directions.

Studies in MHD modelling of the interplanetary environment are incomplete without direct confrontation with observations. It is essential that the MHD models be tested in relation to the "ground truth" provided by solar wind plasma and magnetometer instrumentation aboard spacecraft outside the influence of

9. Burton, R.K., McPherron, R.L., and Russell, C.T. (1975) An empirical relationship between interplanetary conditions and Dst, J. Geophys. Res. 80:4204.

10. Baker, D.N., Hones, Jr., E.W., Payne, J.B., and Feldman, W.C. (1981) A high time resolution study of interplanetary parameter correlations with AE, Geophys. Res. Lett. 8:179-182.

11. Clauer, C.R., McPherron, R.L., Searls, C., and Kivelson, M.G. (1981) Solar wind control of auroral zone geomagnetic activity, Geophys. Res. Lett. 8:915.

12. Holzer, R.E., and Slavin, J.A. (1982) An evaluation of three predictors of geomagnetic activity, J. Geophys. Res. 87:2558-2562.

13. Kamide, Y. (1982) Comment on "An evaluation of three predictors of geomagnetic activity", J. Geophys. Res. (submitted).

14. Kamide, Y., and Akasofu, S.-I. (1982) Notes on the auroral electrojet indices (in press).

Earth's bow shock. We have performed such studies in the past as summarized in several review articles (Dryer;[15-17] Wu[18, 19]) and a doctoral thesis (D'Uston).[6] Further studies with the present quasi-3D model, however, are still needed before it can be used as an operational tool by AWS forecasters. Fortunately, multi-spacecraft observations by the Helios, Voyager, Pioneer, Prognoz-8, ISEE-3, and IMP spacecraft are now being provided by various experimental groups (Burlaga et al;[20-23] Dryer et al;[24] Intriligator;[25] Klein and Burlaga;[26] Richter et al;[27] Zastenker et al;[28] Intriligator and Miller;[29] and Borrini et al.[30]) These groups are delineating properties such as the global extent of flare-generated shock waves, energetic particle modulation, IMF distortions into "magnetic" clouds, and post-shock plasma properties in everincreasing detail. We plan to make comparisons in the future of multi-spacecraft observations with the predictions provided by our MHD model.

Prior to such a massive undertaking, however, it is necessary that general properties of some canonical examples be provided by the model so that major physical properties can be identified. Such is the purpose of the present report. Therefore, we will examine the interplanetary disturbances that are produced by a canonical set of flare-generated shock waves.

2. ANALYSIS

The governing equations for the time-dependent, non-planar MHD problem are mathematical expressions of the physical conservation laws. For convenience of numerical computation, they are written in quasi-conservation form in spherical coordinates and specialized for the equatorial plane ($\theta = 90^{\circ}$). The equatorial plane may be either the ecliptic plane, the solar equatorial plane, or even the equatorial plane in a tilted heliospheric coordinate system. The latter system may also be a candidate for the present analysis as a consequence of the discovery of the solar current sheet (for example, Rhodes and Smith[31]), the empirical study of Zhao and Hundhausen,[32] and the kinematic study of Hakamada and Akasofu.[1] A schematic sketch of heliospheric space is shown in Figure 1a with the two cross-hatched planes indicating the meridional plane and the equatorial plane of our analysis Figure 1b. We will consider a 180° segment of the latter plane.

The general equations for the conservation of fundamental physical quantities (neglecting dissipation, except at shock waves) in mks units are identical to those given by Wu et al[2] and, for completeness, are summarized in Appendix A.

Because of the large number of references cited above, they will not be listed here. See References, page 25.

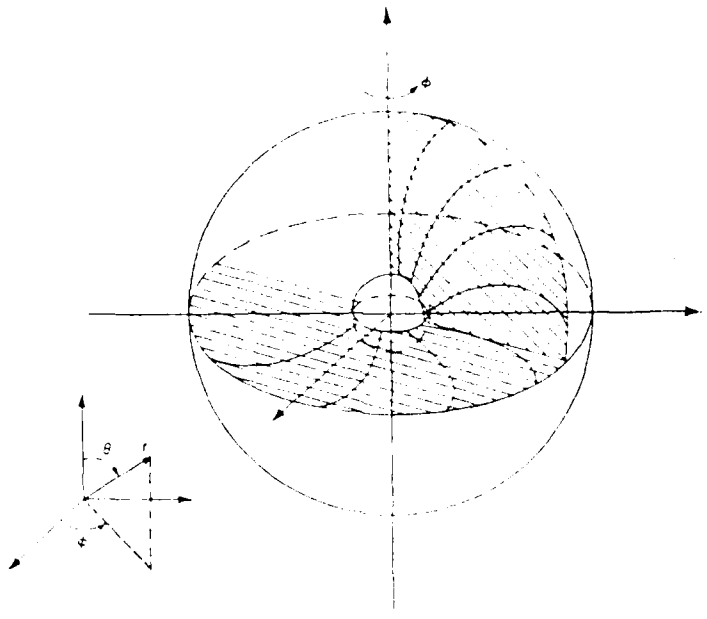

Figure 1a. Illustration of the Spherical Coordinate System and Heliospheric Space. The equatorial plane is chosen for analysis

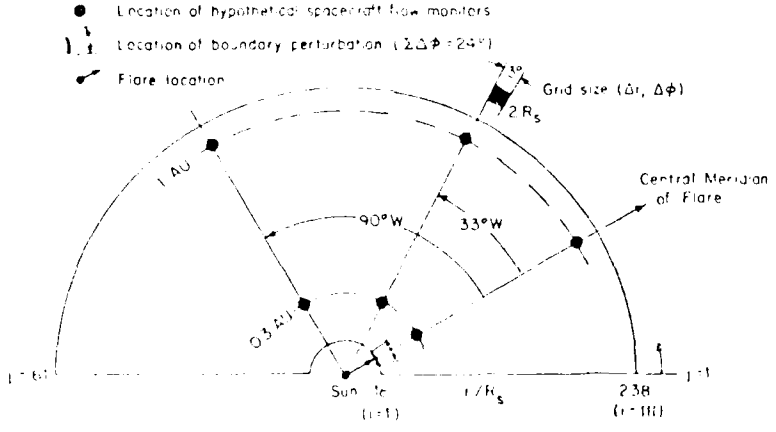

Figure 1b. Schematic Presentation of the Computational Domain, Flare Location at $\phi = 30^{o}$ (Note That $\phi = 0^{o}$ at j = 1), and Positions of Hypothetical Spacecraft Monitors

The ambient steady-state of the interplanetary medium is obtained by setting $\partial(\ )/\partial t \equiv 0$. The result, within our domain of supersonic/super-Alfvénic flow, is a 1-D flow with a canonical Archimedean magnetic-field topology in the equatorial plane (Figure 1a). Initial conditions, including small meridional velocity and magnetic field components, at the inner boundary (taken at 18 R_s, where R_s is the solar radius) are varied until the desired representative values of the various plasma and field parameters are obtained at 1 AU. The parameters at 1.10 AU and at 18 R_s are given in Table 1. The computational domain can be adjusted to suit the particular problem of interest. The present code can handle problems in subsonic as well as in the supersonic flow regime; however, for subsonic flow problems, the boundary conditions should be modified to satisfy the compatibility relations and non-reflective boundary conditions. The latter requirements have been considered in several solar-oriented problems (see, for example, Hu and Wu;[33] and Wu et al.[34]) but not, as yet, in the present code.

Table 1. Initial Steady-State Solar Wind Conditions

Parameter	18 R_s	1.1 AU
n	1.8×10^3 cm^{-3}	10.0 cm^{-3}
V_r	250 km/s	360 km/s
V_θ	0.2 km/s	4.4×10^{-3} km/s
$V\phi$	4.0 km/s	0.5 km/s
B_r	300 nT	2.3 nT
B_θ	1 nT	4.4×10^{-2} nT
B_ϕ	-30.0 nT	-2.0 nT
T	1.1×10^6 °K	3.3×10^4 °K

With respect to grid size, we chose $\Delta r = 2R_s$ and $\Delta\phi = 3^o$. To cover 180^o of heliolongitude and radial distance just beyond 1 AU, 111 radial positions and

33. Hu, Y.Q., and Wu, S.T. (1982) A full-implicit-continuous-Eulerian (FICE) scheme for multidimensional, transient magnetohydrodynamic (MHD) flows, J. Computational Phys. (*in press*).

34. Wu, S.T., Hu, Y.Q., Nakagawa, Y., and Tandberg-Hanssen, E. (1982) Induced mass and wave motions in the lower solar atmosphere. I. Effects of shear motions on flux tubes, submitted to Astrophys. J.

61 azimuthal positions were required (Figure 1b). Smaller grid size would result in better resolution of the flow field at the expense of larger computer storage. Numerical results with the present grid size showed relatively good accuracy.

Each of our solar-flare-generated MHD shock perturbations was introduced at the lower boundary lasting a time, Δt, with a ramp input and decay (to eliminate numerical instability) at each side of the temporal duration. The Rankine-Hugoniot MHD shock jump conditions were separately solved for an arbitrarily-selected shock velocity taking the lower boundary steady state conditions (Table 1) as the pre-shock conditions. The computed post-shock conditions were then taken at the center ($j = 11$) of a 24° longitudinal extent in our equatorial plane. Thus, the shock's central meridian (CM) is located at $\phi = 30^{\circ}$, measured counterclockwise from the horizontal axis in Figure 1b. We assumed a sinusoidal decay of the post-shock conditions to either side of this shock wave in order to simulate the existence of an asymmetrical shock generated originally by our "canonical" solar flare. We will examine global (that is, 180° equatorial plane) snapshots of magnetic field topology, density, and temperature, as well as the time series of the various properties as "measured" by a hypothetical observer at two radial positions, 0.3 AU and 1 AU, along the flare's CM and at two additional heliolongitudinal positions of 33°W and 90°W of the CM (Figure 1b).

Computations were performed for a wide range of shock velocities, V_S, at the center of the arc shown in Figure 1b at $18R_s$: 500, 1000, 1500, 2000, 3000, and 3500 km sec^{-1}. The temporal duration, Δt, of the simulated flare was taken for most of these shock velocities as 1800, 3600, 5400, and 7200 sec. These latter figures are based, rather heuristically, on representative (characteristic) time durations of integrated soft X-ray flux observations by earth-orbiting spacecraft. We will discuss only the case, $V_S = 3000$ sec^{-1} (5400 sec), in this report in order to focus attention on essential physical features of the interplanetary disturbance between the sun and Earth.

3. GENERAL RESULTS

This section will consider some representative, essential results for the case mentioned in Section 2. A detailed examination of the capability of the numerical code to produce physically-relevant additional quantities is given in Appendix B for the same case.

For the purpose of illustration, we will discuss here only the results generated by a "flare" that generates an interplanetary shock wave with a velocity of 3000 km sec^{-1} at 18 solar radii. The temporal duration of this large flare (as

indicated by a hypothetical soft X-ray observation, integrated over the solar disk), is taken to be $\Delta t = 5400$ sec.

Figure 2 shows the contours of total pressure projected onto the solar equatorial plane at t = 0, 20.2, 40.2, and 60.1 hr after initiation of the flare. The contours are labeled by a logarithmic scale for $\text{Log}_{10}\{2nkT + B^2/8\pi\}$ with units of lynes cm^{-2}. The classical Archimedean spiral IMF is not shown at t = 0 hr. It is, however, shown at subsequent times, superimposed upon the total pressure contours, as the flare-generated shock wave expands toward Earth's orbit. We call attention to the local minimum of the total pressure that occurs in the region of the most severe IMF kinking (note the S-shaped reversals). It is clear that this B-field rotation is due to the shock's passage through the solar wind. (Some detailed physics of this feature are discussed in Appendix B.) Yet, within the peripheral areas one detects total pressures that are higher than the earlier undisturbed values at the same locations.

The basic parameter, solar wind velocity, is graphically shown in Figure 3 as an evolving 3-D surface. Only the quadrant $0 < \phi < 90^\circ$, is shown so that the viewer, in inertial space, can observe the disturbance's major features. The undisturbed, steady-state solar wind (homogeneous in heliolongitude) is shown in Figure 3(a). The "cliff" at the lower left corner of each subset of this figure simply represents a discontinuance of the calculation beyond 1.1 AU and, therefore, should be ignored. (We plan to extend the computational domain in the future.) It is seen, in Figure 3(b), that the central, strongest portion of the fast forward shock is about three-fourths of the distance to the earth's orbit. The fast reverse shock's strongest portion is also seen in this figure for t = 20 hr. (Note that the large velocities, as indicated in the figure title, required a scale change from that used in the other parts of the figure.) Attentuation of the shock wave in the heliolongitudinal direction is clearly seen for both fast forward and reverse shocks. Motion of the fast forward shock out of the domain (except for a longitudinal remnant at $\sim\phi$ = 80-90°) is also seen in Figure 3(c). The fast reverse shock passes out of the domain at the later times (~80 hr) as noted in Figure 3(c) and 3(d). As the flow gradually returns to the original steady-state condition, we note several radially-oriented, relatively-higher velocity "ridges" that are clustered around the radially-extended IMF. The ridges represent the loci of several slow mode waves that are the nonlinear counterpart of the well-known "petals" in the Friedrich's phase velocity diagram. It is recalled that the slow mode propagation vectors are restricted in angular extent about the local direction of the magnetic field. Figures 3(e) - 3(g) show the longitudinal motion, away from the original shock's CM, toward both lower and higher values of ϕ.

Figure 4 shows, in a time series format, radial velocity, density, temperature, and IMF total magnitude at 1.0 AU. Figures 4(a) - 4(d) show the time

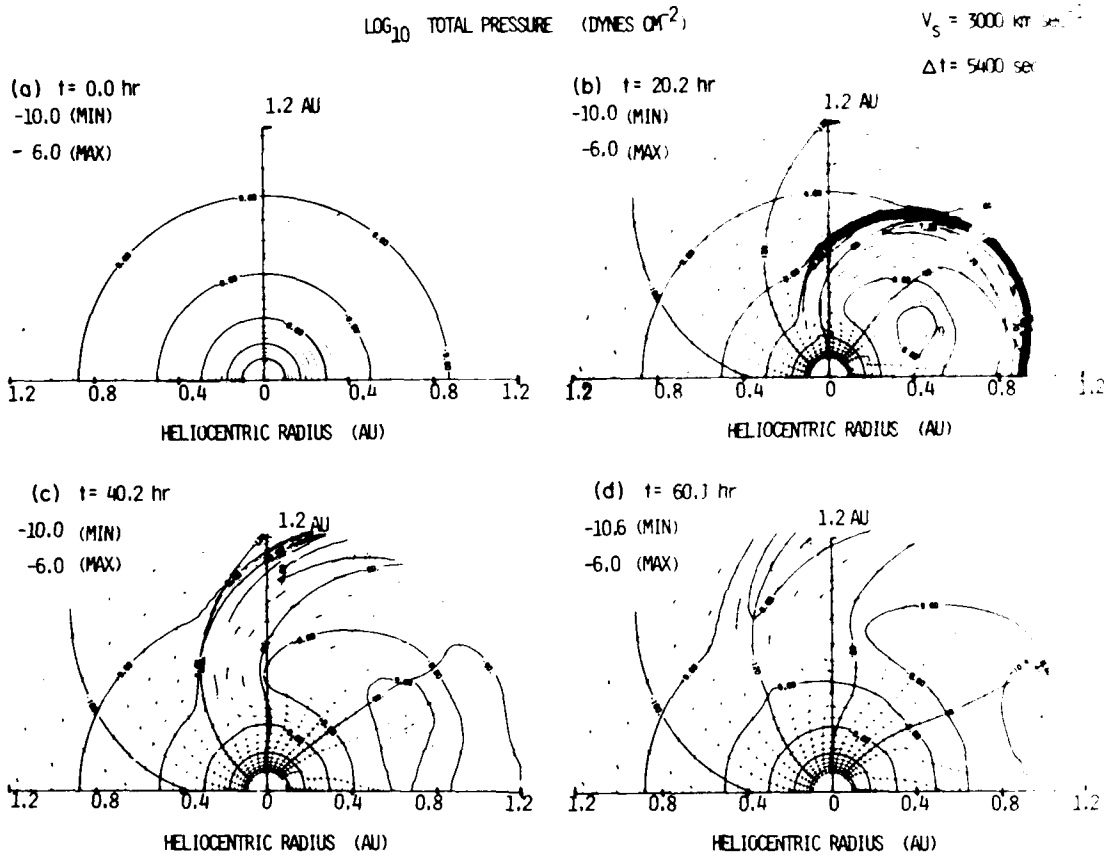

Figure 2. Total Pressure ($2nkT + B^2/8\pi$) Contours, Together with Superposition of Deformed IMF (at $t > 0$ hr), Following Introduction of the Shock Wave, V_S = 3000 km sec^{-1}, Δt = 5400 sec. Numbers are $\log_{10}$ (dynes cm^{-2})

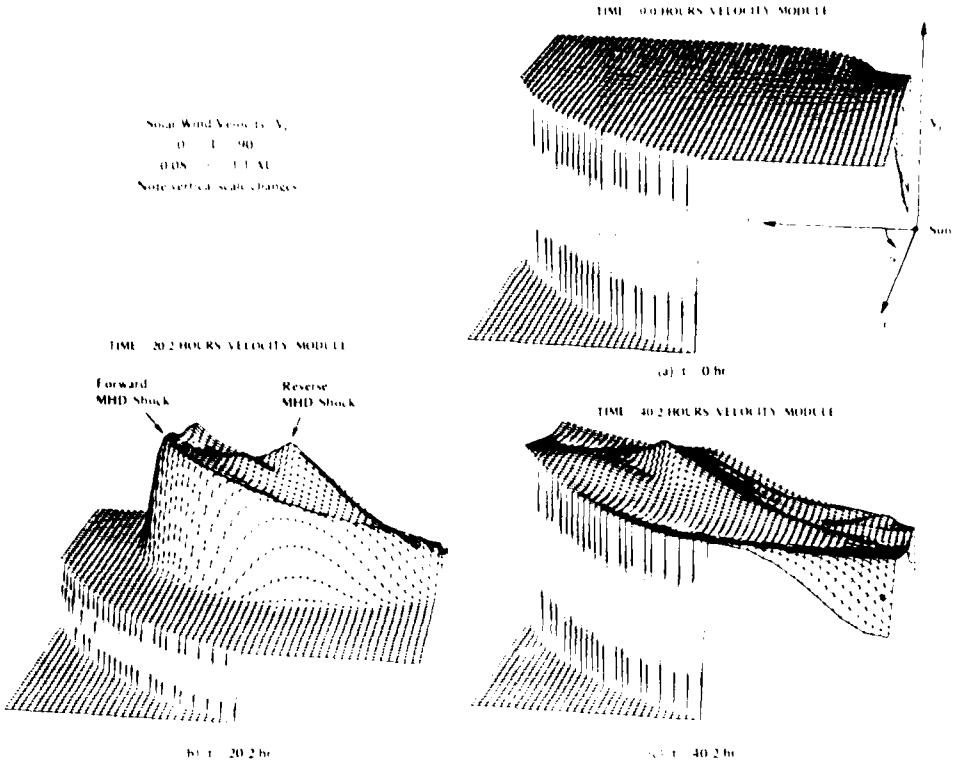

Figure 3. Three-dimensional, Polar, View of the Solar Wind Velocity Surface Within the Quadrant $0 < \phi < 90^{\circ}$. Since the computational domain is terminated at 1.1 AU, the velocity appears as zero outside this distance in this presentation and should, together with the vertical "cliff", be ignored. The outer boundary conditions allow for continuous flow through it as indicated by the smooth passage of, for example, the forward and reverse shocks through r = 1.1 AU: (a) t = 0 hr (ambient, steady-state solar wind as given in Table 1), (b) t = 20 hr [complete structure of the disturbance is contained within the computational domain. Note scale change compared with (a). $(\Delta V)_{max}$ = 618 km sec^{-1}], (c) t = 40 hr [fast forward shock has nearly completed its passage through the 1.1 AU radial position. $(\Delta V)_{max}$ within the computational domain is 383 km sec^{-1}], (d) t = 60 hr [strongest portion of the fast reverse shock is approaching the 1.1 AU radial position. $(\Delta V)_{max}$ = 295 km sec^{-1}], (e) t = 80 hr [strongest portion of the fast reverse shock has passed through the 1.1 AU radial position. $(\Delta V)_{max}$ = 196 km sec^{-1}], (f) t = 100 hr [fast reverse shock has completed its passage through the 1.1 AU radial position. Multiple, radially-aligned "ridges" are remnants, via slow mode wave propagation, of the original disturbances. $(\Delta V)_{max}$ = 100 km sec^{-1}], and (g) t = 160 hr [continuation and gradual attentuation of disturbance and return to ambient conditions. $(\Delta V)_{max}$ = 60 km sec^{-1}]

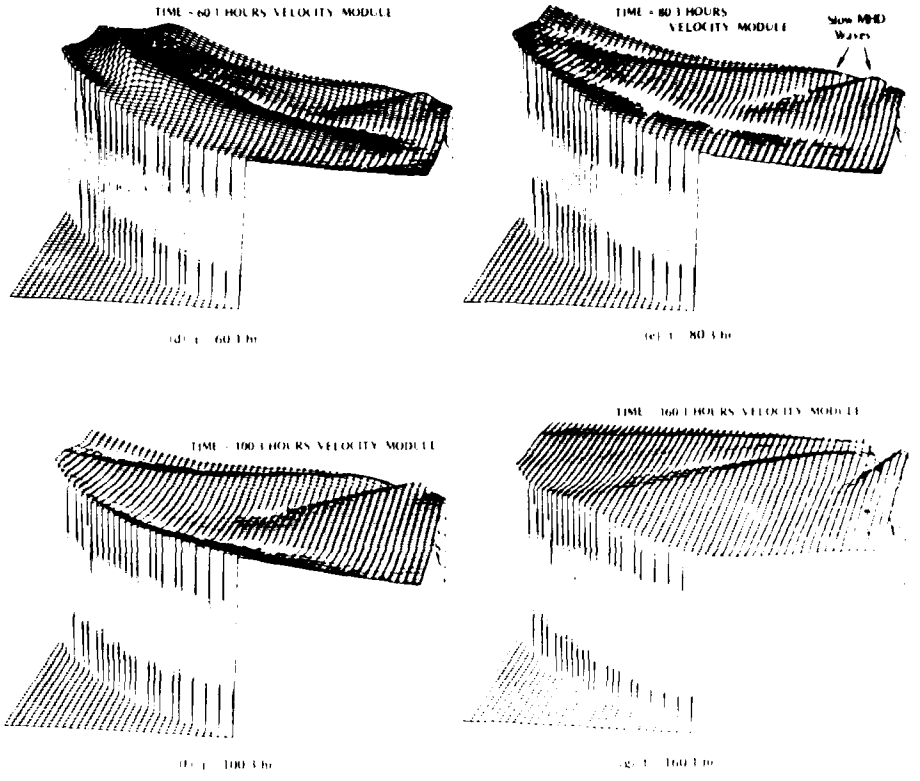

Figure 3. Three-dimensional, Polar, View of the Solar Wind Velocity Surface Within the Quadrant $0 \leq \phi \leq 90^{o}$. Since the computational domain is terminated at 1.1 AU, the velocity appears as zero outside this distance in this presentation and should, together with the vertical "cliff", be ignored. The outer boundary conditions allow for continuous flow through it as indicated by the smooth passage of, for example, the forward and reverse shocks through r = 1.1 AU: (a) t = 0 hr (ambient, steady-state solar wind as given in Table 1), (b) t = 20 hr [complete structure of the disturbance is contained within the computational domain. Note *scale change compared with (a).* $(\Delta V)_{max}$ = *618 km sec*$^{-1}$], *(c) t = 40 hr [fast* forward shock has nearly completed its passage through the 1.1 AU radial position. $(\Delta V)_{max}$ within the computational domain is 383 km sec^{-1}], (d) t = 60 hr [strongest portion of the fast reverse shock is approaching the 1.1 AU radial position. $(\Delta V)_{max}$ = 295 km sec^{-1}], (e) t = 80 hr [strongest portion of the fast reverse shock has passed through the 1.1 AU radial position. $(\Delta V)_{max}$ = 196 km sec^{-1}], (f) t = 100 hr [fast reverse shock has completed its passage through the 1.1 AU radial position. Multiple, radially-aligned "ridges" are remnants, via slow mode wave propagation, of the original disturbances. $(\Delta V)_{max}$ = 100 km sec^{-1}], and (g) t = 160 hr [continuation and gradual attentuation of disturbance and return to ambient conditions. $(\Delta V)_{max}$ = 60 km sec^{-1}] (Contd)

series at the CM of the flare-generated shock pulse. It is seen that the fast forward shock arrives at 1.0 AU at about t = 24 hr and a more well-developed fast reverse shock arrived at about t = 60 hr.

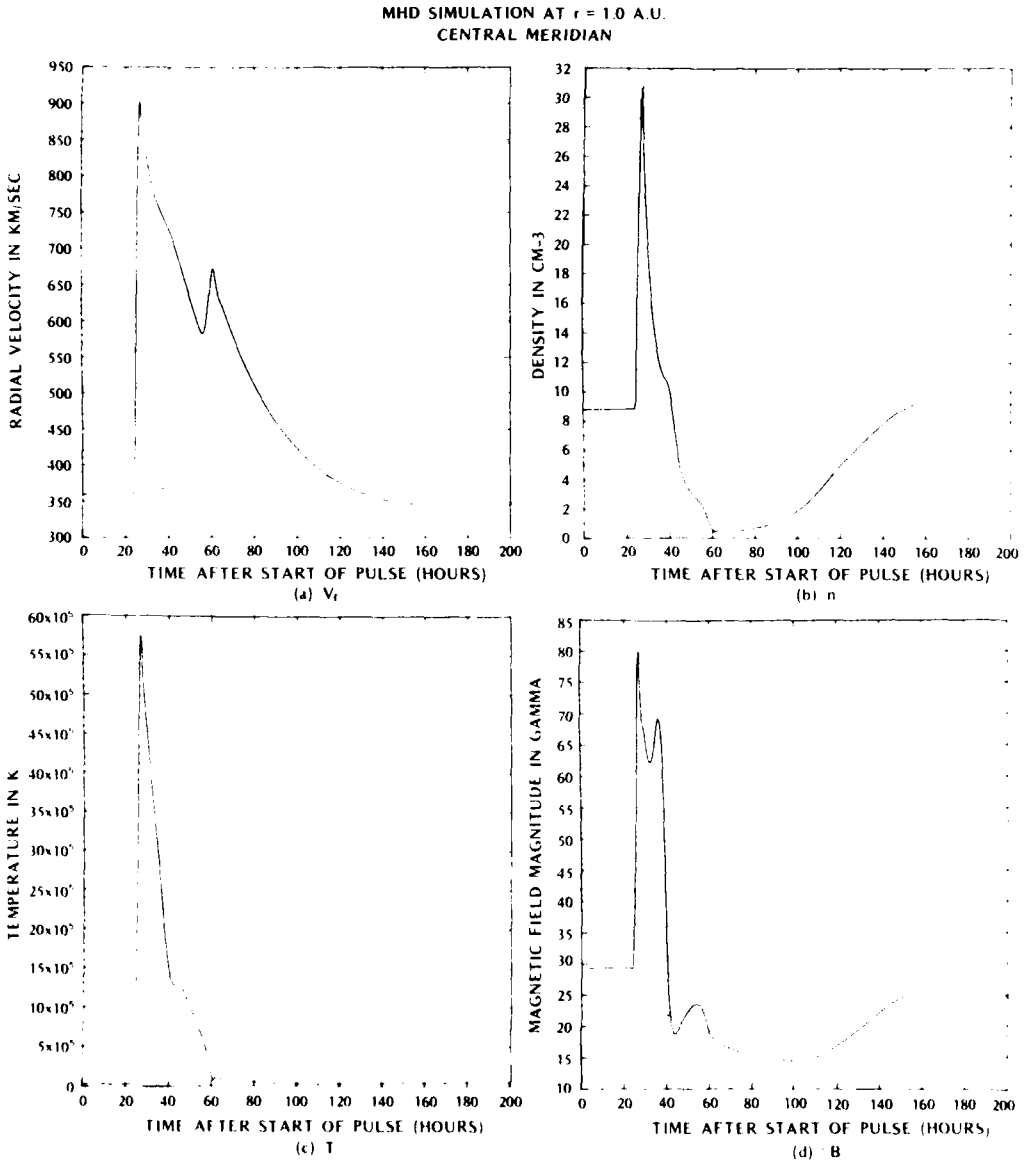

Figure 4. Time Series of Radial Solar Wind Velocity, Density, Temperature, and Total IMF Magnitude at 1.0 AU. CM of flare-generated shock (a-d)

4. GEOPHYSICALLY-RELEVANT SOLAR WIND PARAMETERS

As noted in the Introduction, there is currently an evaluation of various combinations of solar wind parameters and their statistical relevance in regard to various geomagnetic indices. We have already implicitly answered the first of the four fundamental questions posed in the Introduction. We have done so, at least, for the case considered thus far: a uniform steady-state solar wind with a canonical spiral IMF that is disturbed by a very fast shock at $18R_S$, namely the case of $V_S = 3000$ km sec^{-1}, $\Delta t = 5400$ sec. Thus, if the earth were located at or within 90°W of the pulse's CM, we would reply in the affirmative to the question: Will a disturbance (presumed to be known with some confidence close to the sun) reach the earth? We will study the case of larger angles, both west and east of the CM in the future.

The second question is, if a disturbance will reach the earth's magnetosphere, when will it begin? Arrival of the fast-forward shock wave at the magnetosphere will produce a storm sudden commencement. (Whether a storm main phase will follow is discussed later.) We have intensively examined the case mentioned in the preceding paragraph. As noted earlier, we also studied a wide range of initial shock velocities and flare duration times. The range of initial velocities was $500 \leq V_S \leq 3500$ km sec^{-1} and $3600 < \Delta t < 7200$ sec. As noted, details of the disturbed plasma and IMF for most of these cases are given in Appendix B. The upper limit for transit time is that given for the case of the original steady-state solar wind. Thus, the integrated transit time for a test particle moving at 250 km sec^{-1} at $18R_S$ (Table 1) is 110 hr in all directions (since CM in this limiting case has no meaning). A test particle moving faster than this speed will obviously arrive sooner at 1 AU. Thus, a small pulse that produces only the three well-known MHD (fast, slow, and Alfvén) modes will not produce a fast shock until the disturbance velocity exceeds the fast mode. Our lowest V_S exceeds this bound; we have not studied (here) the case of purely linear, or even nonlinear, MHD wave modes and their coupling (although our computer code is fully capable of handling such situations). Thus, strictly speaking, our results for shock transit time, shown in Figures 5(a) - 5(c), apply only to the fast-forward shock wave. The curves' upper bound is simply the 110-hr transit time for the undisturbed steady-state solar wind. The curves have been extrapolated to $V_S = 4500$ km sec^{-1} as part of our polynomial fits to the individual points found from our more restricted study.

We made no attempt to extrapolate below or above the assumed set of "flare duration" times, Δt. Classically, a shock wave that results from a delta function input of energy is called a "blast wave". (We leave the interpolation of this case, $\Delta t \to 0$, to the reader.) Rigorously, then, all of our shocks are really

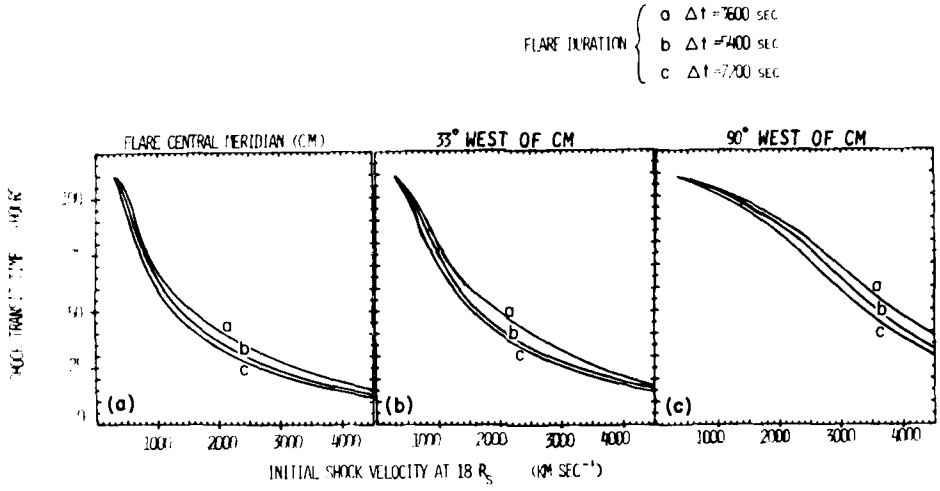

Figure 5. Shock Transit Time to 1.0 AU. The initial shock velocity is assumed to be known at $18R_S$; no allowance is made for the transit time from 1.0 - $18R_S$. The "flare duration" time is assumed to be known, on a heuristic basis from the temporal profile of the soft X-ray flux (for example, 1-8Å) from a given flare: (a) CM, (b) 33°W of the CM, and (c) 90°W of CM

"piston-driven" shocks because Δt is finite. Since our choices for Δt are small relative to the transit times for most of our V_s choices, we would be justified in referring to these shocks as "blast waves" only after Δt has been completed and the elapsed time is large compared with Δt. As a counter example, for the case of $V_s >> 3500$ km sec^{-1} and $\Delta t > 7200$ sec, and at CM, the shock transit time will be of order of 10 hr. If Δt were of order of 3 to 5 hr, we should refer to such a shock as "piston-driven" all the way to 1 AU. In any case, Figure 5 provides a prediction (neglecting an additional, but small, correction for the transit time from 1-$18R_s$) for the second, operationally-motivated, question: when will the disturbance (read: fast forward shock for our study) reach earth? A final caveat is important: Figure 5 pertains only to the representative solar wind velocity profile given in Table 1, thus the transit times for other cases would require revision upward or downward!

The third and fourth questions posed in the Introduction (how severe? how long?) are much more difficult to answer for the general case of spatially-inhomogeneous photospheric, coronal and solar wind conditions, at best, and for the temporal changes that are superimposed on such a background, at worst. We will return to our "ansatz" or "canonical" example of the case $V_s = 3000$ km sec^{-1} ($\Delta t = 5400$ sec) in order to offer straightforward answers to these two questions. Our answers are obtained self-consistently from the foregoing results

within the context of the somewhat controversial debate currently underway as noted in the Introduction. We will, therefore, discuss our calculations for the energy flux parameter, ϵ, and the electric field, VB_s. Note that the former is evaluated in the frame of solar-ecliptic coordinates (*not solar-magnetospheric* coordinates). Note, also, that our velocity is the resultant magnitude of the velocity (which coincides with other current usage). Our "B_z" is really B_θ, which is positive when directed southward (by virtue of our use of standard spherical coordinates). Since B_z, as used by magnetospheric physicists, is negative when directed southward of the ecliptic, the reader is asked to change signs (mentally) when comparing these results with those shown in magnetospheric papers on this subject.

Figure 6 shows the time series for ϵ and VB_θ at 1.0 AU for the case: V_s = 3000 km sec^{-1}, Δt = 5400 sec. If we were to adopt the recipe proposed, for example, by Hakamada and Akasofu,[1] we would predict high latitude activity, as measured by the AE index, to commence at t = 24 hr (immediately following the SC) when ϵ rises to the first threshold of 10^{18} erg sec^{-1}. We assume, for this exercise, that the earth's magnetosphere is located at CM. The second threshold of 10^{19} erg sec^{-1} would be breached at t ~ 26 hr when the magnetospheric ring current would develop, as measured by Dst, and the main phase of the geomagnetic storm would begin with associated auroral zone motion and ionospheric disturbances at lower latitudes. Interpreting the 10^{19} erg sec^{-1} threshold somewhat liberally, we might suggest that the Dst would fluctuate somewhat until t ~ 38 hr, at which time the low to medium latitudes would recover to pre-storm conditions. The high latitude activity would persist until ϵ falls below 10^{18} erg sec^{-1} at t ~ 57 hr. Overall, then, one would suggest, on the basis of this exercise, that the activity (when earth is located at CM) would primarily be located at high latitudes, with a brief Dst perturbation. As for the fourth question, a time duration of 57-24 = 33 hr would be offered as a prediction for the storm's duration.

On the other hand, if we were to adopt the concept of the half-wave rectifier proposed, for example, by Burton et al,[9] we would predict AE activity commencing (as in the previous example) at t ~ 24 hr and ending at t ~ 31 hr when VB_θ in Figure 6 is positive (negative, in the parlance of the magnetospheric physicists). The large negative values in Figure 6 would, in this recipe, not be relevant since the B_z component (B_θ in our parlance) would be northward during the interval 31 < t < 60 hr.

Clearly, these two recipes discussed would also be used for the most probable cases when the earth's magnetosphere is at locations other than CM. We hope it is clear to the reader that location relative to CM is not necessarily the prime consideration. The strength of the perturbation (velocity) as well as the

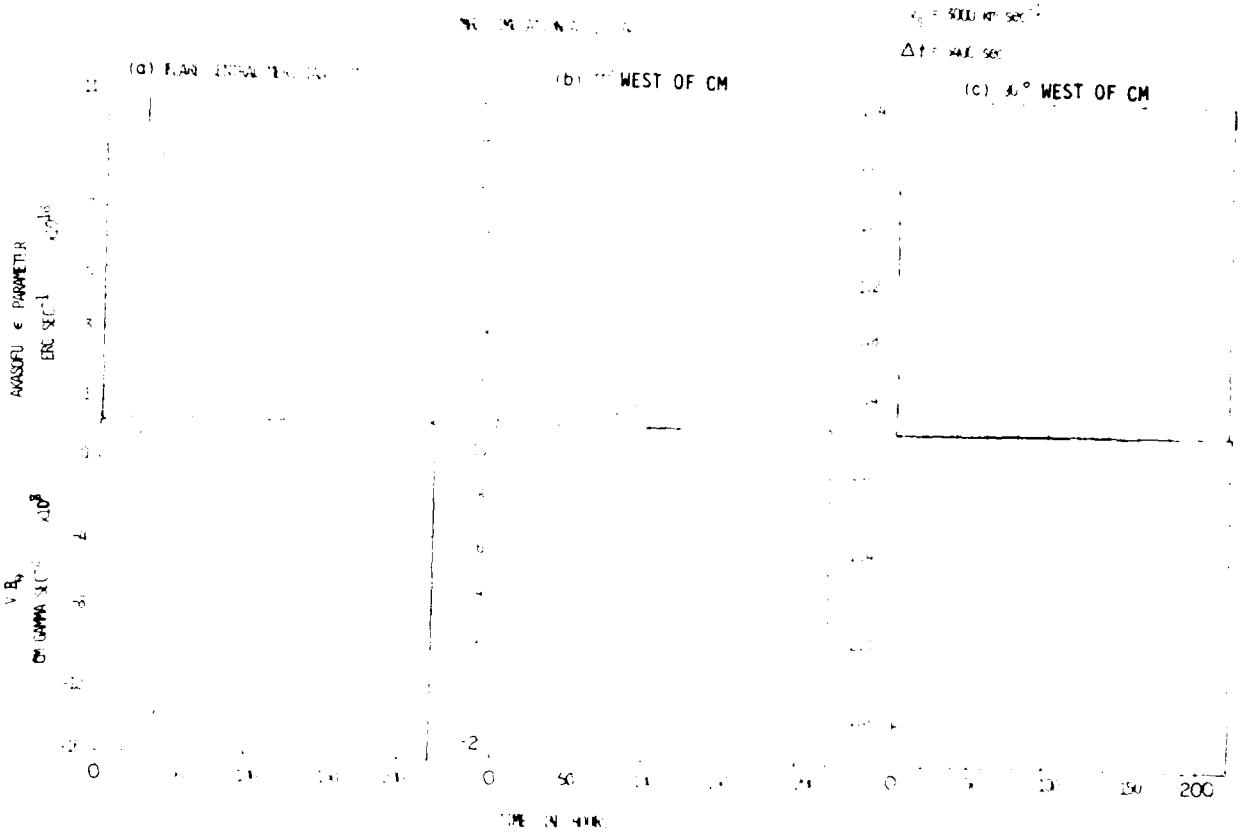

Figure 6. Energy Flux Parameter, ϵ, and the Product VB_θ at 1 AU for the Case Vs = 3000 km sec^{-1}, Δt = 5400 sec. (a) CM, (b) 33°W of CM, and (c) 90°W of CM

orientation of the B_θ component evolve in the earthward direction following some kind of change at the sun. Hence, it is possible (as shown for the 33°W position in the central panel of Figure 6) that ϵ can be greater at positions other than CM.

5. CONCLUDING REMARKS

We have used a time-dependent, nonplanar, 2-D MHD computer model to simulate a number of flare-generated shock waves and their concomitant effects on the interplanetary medium. The example of $V_s \simeq 3000$ km sec^{-1}, with an assumed flare (or, equivalently, energy input) time of 5400 sec, was used as a detailed illustrative case. A representative steady-state, solar wind with axial symmetry, was assumed for simplicity as part of this "ansatz" problem with three components of the velocity vector and magnetic field. Hence, all nonlinear wave mode coupling is included self-consistently.

The following major result evolved from the presentation of the complete sets of plasma and IMF parameters. We have established the fact that the model can be satisfactorily used to compute any form of geophysically-relevant solar wind parameter (such as ϵ or VB_s) for long-range ($\sim$ days) predictions of geomagnetic and ionospheric activity. Future work must include retrospective tests that employ both solar and multi-spacecraft observations for specific intervals of time. Perhaps several weeks before, during, and after one or more solar flares and/or coronal hole evolutionary observations should be a minimum temporal range that should be used in a test made for the MHD model.

Still lacking in the present work is the incorporation of additional physical phenomena such as multi-fluids, dissipation (thermal conduction, viscosity, and electrical resistivity), and more initial-boundary value conditions that are more realistically reflective of the changing mood of solar conditions. Perhaps the two most important omissions in the present work are the incorporation of hybrid kinetic/fluid effects as discussed by Cuperman[35] and Wu[19] and more realistic considerations of heat flux and non-Maxwellian distribution functions. Last, but not least, even the most "primitive" version of the MHD model as discussed here, must be tested by direct confrontations with a number of spacecraft observations during specific (that is, not statistical) intervals of solar/interplanetary activity.

35. Cuperman, S. (1982) Solar wind theory, Space Sci. Rev. (in press).

References

1. Hakamada, K., and Akasofu, S. I. (1982) Simulation of three-dimensional solar wind disturbances and resulting geomagnetic storms, Space Sci. Rev. 31:3-70.

2. Wu, S. T., Dryer, M., and Han, S. M. (1982) Non-planar MHD model for solar flare-generated disturbances in the heliospheric equatorial plane, submitted to Solar Physics.

3. Wu, S. T., Han, S. M., and Dryer, M. (1979) Two-dimensional, time-dependent MHD description of interplanetary disturbances: simulation of high speed solar wind interactions, Planet. Space Sci. 27:255-264.

4. Dryer, M., Wu, S. T., and Han, S. M. (1980) Two-dimensional, time-dependent MHD simulation of the disturbed solar wind due to representative flare-generated and coronal hole-generated disturbances, Geofis. Intern. 19:1-15.

5. D'Uston, C., Dryer, M., Han, S. M., and Wu, S. T. (1981) Spatial structure of flare-associated perturbations in the solar wind simulated by a two-dimensional numerical MHD model, J. Geophys. Res. 86:525-534.

6. D'Uston, C. (1981) Dynamique des Ondes de Choc Interplanetaires Engendrees par des Eruptions Solaires, PhD thesis in Physical Sciences, University Paul Sabatier de Toulouse, Toulouse, France.

7. Smart, D. F., Garrett, H. B., and Shea, M. A. (1980) The prediction of AE, ap, and Dst at time lags between 0 and 30 hours, in Solar-Terrestrial Predictions Proceedings, Vol. II, R. F. Donnelly, Ed., U. S. Government Printing Office, Washington, D. C., pp. 399-413.

8. Perreault, P., and Akasofu, S.-I. (1978) A study of geomagnetic storms, Geophys. J. R. Astr. Soc. 54:547.

9. Burton, R. K., McPherron, R. L., and Russell, C. T. (1975) An empirical relationship between interplanetary conditions and Dst, J. Geophys. Res. 80:4204.

10. Baker, D.N., Homes, Jr., E.W., Payne, J.B., and Feldman, W.C. (1981) A high time resolution study of interplanetary parameter correlations with AE, Geophys. Res. Lett. 8:179-182.

11. Clauer, C.R., McPherron, R.L., Searls, C., and Kivelson, M.G. (1981) Solar wind control of auroral zone geomagnetic activity, Geophys. Res. Lett. 8:915.

12. Holzer, R.E., and Slavin, J.A. (1982) An evaluation of three predictors of geomagnetic activity, J. Geophys. Res. 87:2558-2562.

13. Kamide, Y. (1982) Comment on "An evaluation of three predictors of geomagnetic activity", J. Geophys. Res. (submitted)

14. Kamide, Y., and Akasofu, S.-I. (1982) Notes on the auroral electrojet indices (in press).

15. Dryer, M. (1974) Interplanetary shock waves generated by solar flares, Space Sci. Rev. 15:403-468.

16. Dryer, M. (1975) Interplanetary shock waves: Recent developments, Space Sci. Rev. 17:277-325.

17. Dryer, M. (1982) Coronal transient phenomena, Space Sci. Rev. (in press).

18. Wu, S.T. (1980) Theoretical interpretation of travelling interplanetary phenomena and their solar origins, in Solar and Interplanetary Dynamics, Proc. of IAU Symposium No. 91, M. Dryer and E. Tandberg-Hanssen, Eds., D. Reidel Publ. Co., Boston, Mass., pp. 443-458.

19. Wu, S.T. (1982) Propagation of solar disturbances: theory and models, Space Sci. Rev. (in press).

20. Burlaga, L.F., Ness, N.F., Mariani, F., Bavassano, B., Villante, U., Rosenbauer, H., Schwenn, R., and Harvey, J. (1978) Magnetic fields and flows between 1 and 0.3 AU during the primary mission of Helios 1, J. Geophys. Res. 83:5167.

21. Burlaga, L.F., Lepping, R., Weber, R., Armstrong, T., Goodrich, C., Sullivan, J., Gurnett, D., Kellogg, P., Keppler, E., Mariani, F., Neubauer, F., Rosenbauer, H., and Schwenn, R. (1980) Interplanetary particles and fields, November 22 - December 6, 1977: Helios, Voyager, and IMP observations, J. Geophys. Res. 85:2227-2242.

22. Burlaga, L.F., Sittler, E., Mariani, F., and Schwenn, R. (1981) Magnetic loop behind an interplanetary shock: Voyager, Helios, and IMP 8 observations, J. Geophys. Res. 86:6673-6684.

23. Burlaga, L.F., Lepping, R.P., Behannon, K.W., Klein, L.W., and Neubauer, F.M. (1982) Large-scale variations of the interplanetary magnetic field: Voyager 1 and 2 observations between 1-5 AU, J. Geophys. Res. 87:4345-4353.

24. Dryer, M., Candelaria, C., Smith, Z.K., Steinolfson, R.S., Smith, E.J., Wolfe, J.H., Mihalov, J.D., and Rosenau, P. (1978) Dynamic modelling of the solar wind disturbances during the August 1972 events, J. Geophys. Res. 83:532-540.

25. Intriligator, D.S. (1980) Transient phenomena originating at the sun - an interplanetary view, in Solar and Interplanetary Dynamics, Proc. of IAU Symposium No. 91, M. Dryer and E. Tandberg-Hanssen, Eds., D. Reidel Publ. Co., Dordrecht, pp. 357-374.

26. Klein, L.W., and Burlaga, L.F. (1982) Interplanetary magnetic clouds at 1 AU, J. Geophys. Res. 87:613-624.

27. Dubinin, A.K., Verigin, M.I., Kurt, V.G., Stolpovsky, V.G., Gringauz, K.I., Keppler, E., Rosenbauer, H., Neubauer, F.M., Gombosi, T., and Somogyi, A. (1981) The 3 January 1978 interplanetary shock event as observed by energetic particle, plasma and magnetic field devices on board of HELIOS-1, HELIOS-2 and PROGNOZ-6, J. Geophys. 50:101-109.

28. Zastenker, G., Vaisberg, O.L., Balebanov, V.M., Omelchenko, A.N., Nozdrachev, M.N., Yermolaev, Y.I., Klimov, S.I., and Borodkova, N.L. (1982) Dynamics of solar wind plasma parameters and behavior of magnetospheric boundaries during the arrival of interplanetary shock waves to the Earth in the events of April - May, 1981, in Proceedings of SCOSTEP/STIP Symposium on Solar/Interplanetary Intervals, S. McKenna-Lawlor, M.A. Shea, and D.F. Smart, Eds., Royal Irish Academy, Dublin (in press).

29. Intriligator, D.S., and Miller, W.D. (1982) Plasma shocks and energetic particles in the outer solar system: Trapping and asymmetry observations from Pioneer 10 and Pioneer 11, J. Geophys. Res. 87:4354-4364.

30. Borrini, G., Gosling, J.T., Bame, S.J., and Feldman, W.C. (1982) An analysis of shock wave disturbances observed at 1 AU from 1971 through 1978, J. Geophys. Res. 87:4365-4373.

31. Rhodes, Jr., E.J., and Smith, E.J. (1981) Multi-spacecraft observations of heliographic latitude-longitude structure in the solar wind, J. Geophys. Res. 86:8877.

32. Zhao, X.-P., and Hundhausen, A.J. (1981) Organization of solar wind plasma properties in a tilted, heliomagnetic coordinate system, J. Geophys. Res. 86:5423-5430.

33. Hu, Y.Q., and Wu, S.T. (1982) A full-implicit-continuous-eulerian (FICE) scheme for multidimensional, transient magnetohydrodynamic (MHD) flows, J. Computational Phys. (in press).

34. Wu, S.T., Hu, Y.Q., Nakagawa, Y., and Tandberg-Hanssen, E. (1982) Induced mass and wave motions in the lower solar atmosphere. I. effects of shear motions on flux tubes, submitted to Astrophys. J.

35. Cuperman, S. (1982) Solar wind theory, Space Sci. Rev. (in press).

Appendix A

General Equation for the Conservation of Fundamental Physical Quantities

The governing equation for the conservation of fundamental physical quantities without dissipation (except at shock waves) in mks units is;

$$\frac{\partial \underline{W}}{\partial t} + \frac{\partial \underline{F}}{\partial r} + \frac{1}{r}\frac{\partial \underline{G}}{\partial \phi} = \underline{S} \tag{A1}$$

where

$$\underline{W} = \begin{bmatrix} r^2\rho \\ r^2\rho V_r \\ r^2\rho V_\theta \\ r^2\rho V_\phi \\ rB_r \\ rB_\theta \\ rB_\phi \\ r^2 E \end{bmatrix} \tag{A2}$$

$$\underline{F} = \begin{bmatrix} r^2 \rho V_r \\ r^2 \left(p + \rho V_r^2 + \frac{-B_r^2 + B_\theta^2 + B_\phi^2}{2\mu_o} \right) \\ r^2 \left(\rho V_r V_\theta - \frac{B_r B_\theta}{\mu_o} \right) \\ r^2 \left(\rho V_r V_\phi - \frac{B_r B_\phi}{\mu_o} \right) \\ 0 \\ r \left(V_r B_\theta - V_\theta B_r \right) \\ r \left(V_r B_\phi - V_\phi B_r \right) \\ r^2 \left\{ V_r \left[\frac{\gamma}{\gamma - 1} p + \frac{1}{2} \rho |\underline{V}|^2 \right] + \frac{B_\theta}{\mu_o} \left[V_r B_\theta - V_\theta B_r \right] - \right. \\ \left. - \frac{B_\phi}{\mu_o} \left[V_\phi B_r - V_r B_\phi \right] \right\} \end{bmatrix} \qquad \text{(A3)}$$

$$\underline{G} = \begin{bmatrix} r^2 \rho V_\phi \\ r^2 \left(\rho V_r V_\phi - \frac{B_r B_\phi}{\mu_o} \right) \\ r^2 \left(\rho V_\theta V_\phi - \frac{B_\theta B_\phi}{\mu_o} \right) \\ r^2 \left(p + \rho V_\phi^2 + \frac{B_r^2 + B_\theta^2 - B_\phi^2}{2\mu_o} \right) \\ r \left(V_\phi B_r - V_r B_\phi \right) \\ r \left(V_\phi B_\theta - V_\theta B_\phi \right) \\ 0 \\ r^2 \left\{ V_\phi \left[\frac{\gamma}{\gamma - 1} p + \frac{1}{2} \rho |\underline{V}|^2 \right] + \frac{B_r}{\mu_o} \left[V_\phi B_r - V_r B_\phi \right] - \right. \\ \left. - \frac{B_\theta}{\mu_o} \left[V_\theta B_\phi - V_\phi B_\theta \right] \right\} \end{bmatrix} \qquad \text{(A4)}$$

and

$$\underline{S} = \begin{bmatrix} 0 \\ 2rp + r^2\rho \frac{\partial \psi}{\partial r} + \frac{rB_r^2}{\mu_o} + \rho r (V_\theta^2 + V_\phi^2) \\ \frac{rB_r B_\theta}{\mu_o} - \rho r V_r V_\theta \\ \frac{rB_r B_\phi}{\mu_o} - \rho r V_r V_\phi \\ 0 \\ 0 \\ 0 \\ r^2 \rho V_r \frac{\partial \psi}{\partial r} \end{bmatrix} \tag{A5}$$

where

$$E = \left(\frac{1}{\gamma - 1} p + \frac{1}{2} \rho |\underline{V}|^2 + \frac{|\underline{B}|^2}{2\mu_o} \right) \tag{A6}$$

$$p = 2\rho RT \tag{A7}$$

$$\psi = \frac{M_S G}{r} \tag{A8}$$

The first term in Equations (2) - (5) gives the continuity equation for conservation of mass. The second, third, and fourth terms give the momentum equations in the radial, meridional, and azimuthal directions, respectively. The fifth, sixth, and seventh terms give the induction equation in the same three directions [again, $\partial(\ )/\partial\theta \equiv 0$] with infinite electric conductivity governing the coupled interaction between the plasma motion and the magnetic field. Finally, the eighth term provides the energy-conservation equation for our one-fluid system. This dynamic system is assumed to be adiabatic and the symbols have their usual meaning: ρ is the mass density; $\underline{V} = (V_r, V_\theta, V_\phi)$ denotes the mass-flow velocity vector; T is the temperature; $\underline{B} = (B_r, B_\theta, B_\phi)$ denotes the magnetic field; $p = 2\rho RT$ is the gas pressure, accounting for equal electron and proton contributions via

Dalton's law; M_s is the solar mass; Ψ the gravitational potential; G the gravitational acceleration at the surface of the Sun ($r = R_s$); γ the specific heat ratio (5/3); and μ_o is the magnetic permeability in a vacuum. The independent variables are time (t) and the radial (r) and azimuthal (ϕ) coordinates in this non-planar (2-D, 3-component) system.

Appendix B

Additional Results

We have presented major results in the main text for the case: V_s = 3000 km sec^{-1}, Δt = 5400 sec. In order to examine the more detailed physics, for completeness we shall now outline some other interesting results in this appendix for this case. The capability of the MHD model to provide temporal and spatial details of the disturbed interplanetary plasma and IMF will also be demonstrated.

Figure B1 shows the IMF as projected into the equatorial plane at t = 0, 20.2, 40.2, and 60.1 hr. Recalling the location of the shock's CM (equivalent, essentially, to the flare's CM), we note the fast forward shock-induced deformation, particularly along and east of the CM. Of particular interest is the reversed IMF polarity (from outward to inward) within the disturbed flow at t = 40.2 hr. We will refer again to this feature and the physical mechanism with which this kinking is associated. As the shock recedes into the far reaches (that is, beyond 1 AU in the present case) of the equatorial plane, the IMF gradually returns (t = 200 hr) to its pre-flare Archimedean topology. The numbers on the heavier lines are constants associated with magnetic vector potential; they have no meaning other than their usefulness in the identification (as time progresses) of the footpoint of a particular field line at $18R_s$. These field lines have already been shown, in Figure 2, superimposed upon the total pressure contours. Here in Figure B1, however, the distorted IMF can be seen more clearly.

Figure B2 shows the contours of $Log_{10}T$ together with the superimposed IMF from the previous figure. The formation of the fast forward MHD shock wave is

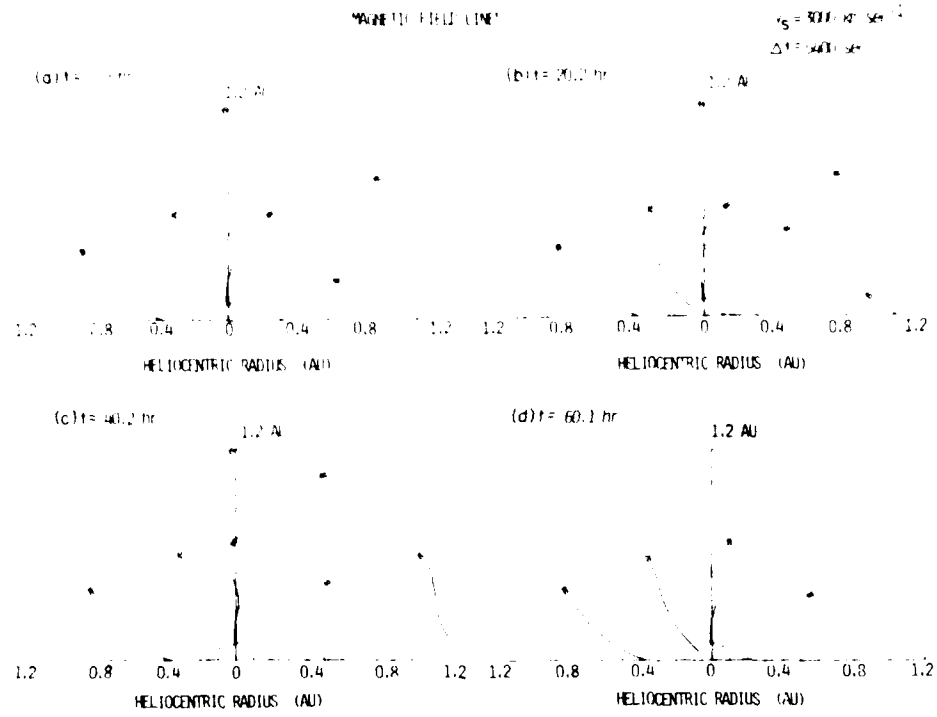

Figure B1. Interplanetary Magnetic-field Line Deformation Following Introduction of a Solar Flare-generated Shock Wave, V_S = 3000 km sec^{-1} and Δt = 5400 sec. (a) t = 0 hr, (b) t = 20.2 hr, (c) t = 40.2 hr, and (d) t = 60.1 hr. The numbers on the heavier lines are chosen by the computer (from the vector potential constants) and indicate the original longitudinal position at $18R_S$

now observed more clearly. We can also observe the formation (between the contours along the CM within the values at t = 20.2 hr, $Log_{10}T$ = 6.0 and 6.4) of a fast reverse MHD shock wave. See also D'Uston et al, [B1] where this formation was described in more detail. At t = 40.2 hr, the shock is identified between the contours of $Log_{10}T$ = 5.6 and 6.0. The reverse shock reaches 1 AU at about t = 60.1 hr. Note that the forward shock becomes attenuated as the position angle of an observer increases to each side of the CM. The reverse shock is much narrower; it too becomes attenuated at much smaller position angles. It is of great importance to emphasize the substantial amount of heliolongitudinal

B1. D'Uston, C., Dryer, M., Han, S. M., and Wu, S. T. (1981) Spatial structure of flare-associated perturbations in the solar wind simulated by a two-dimensional numerical MHD model, J. Geophys. Res. 86:525-534.

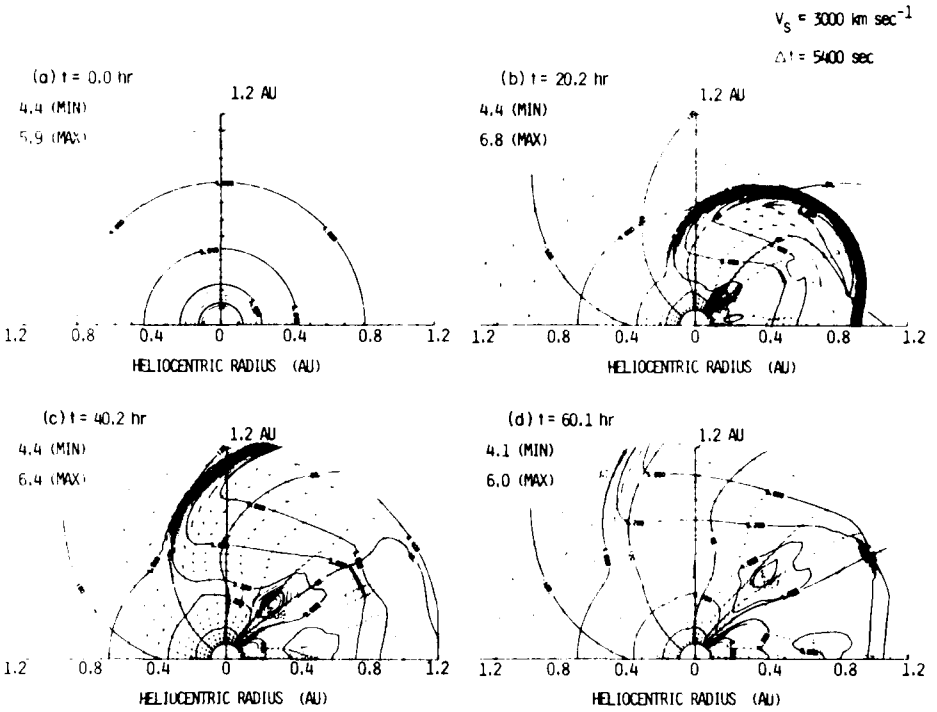

Figure B2. Temperature Contours, Together With Superposition of Deformed IMF (at t > 0 hr), Following Introduction of the Shock Wave, V_S = 3000 km sec^{-1}, Δt = 5400 sec. Numbers are $\log_{10}$ (°K)

spreading (beyond 90°) accomplished by the shock whose original "angle of spread" at 18R_S was only 24°. It is also of great interest to note that the region of IMF polarity reversal (t = 40.2 hr) takes place in the vicinity of the reverse shock. We believe that, for the present case, the reverse shock is a parallel shock where the plasma temperature gradient is the steepest, hence there is no introduction of an azimuthal IMF component. At $\phi < 30°$ (that is, east of the flare's CM) the reverse shock is quasi-parallel, hence an azimuthal IMF is required on the downstream (anti-sunward) side of the shock. The subsequent bending of the IMF must be compatible with the azimuthal component generated by the eastward flank of the fast forward shock (outside the computational domain at t = 40.2 hr). The net result is the spatially-deformed IMF as shown near (and eastward of) the CM in Figure B2(c).

Before leaving the temperature contours, we wish to point to another important result: the outward movement near CM of a region of temperatures that are

cooler than the pre-disturbed values at the same points. We call the readers' attention to the contours that intrude, as it were, sunward from the local minimum. As time progresses, these sunward contour "intrusions" become more elongated. It can be seen, by comparison with the contours for t = 0 hr [Figure B2(a)] that the temperatures are indeed cooler than their undisturbed values along this narrow heliolongitudinal corridor.

We have called this IMF and temperature behavior to the readers' attention because of its relevance to the observations of magnetic "clouds" (Klein and Burlaga;[B2] Burlaga et al.,[B3] and others). We will return to this point in several additional discussions, regarding the density, total pressure, and plasma beta ($\beta = 16\pi\, nkT/B^2$).

Figure B3 shows the contours of $Log_{10}n$ (cm^{-3}) together with the superimposed IMF from Figure B1. The large extent of the low density, overexpanded regions behind the fast forward MHD shock has been pointed out in earlier work (Wu, Han, and Dryer;[B4] Dryer, Wu, and Han;[B5] and D'Uston et al.[B1]) and is evident here again. Here, however, we can relate particularly-low minima with the IMF twists and turns as outlined during the temperature discussion.

We also call attention to contours of plasma beta ($\beta = 16\pi\, nkt/B^2$) in Figure B4. This parameter is of importance, not only in the context of discussions of the magnetic clouds (Klein and Burlaga;[B2] Burlaga et al.[B3]), but also in the study of the structure and foreshock characteristics of both forward and reverse shocks. Plasma β (ratio of thermal to magnetic pressures) is also of great importance in the eventual delineation of a hybrid linkage of kinetic and MHD modelling of interplanetary disturbances in a self-consistent way. Figures B4(b) and B4(c) clearly show the attainment of extremely-large values of $\beta >> 1$ that are co-spatial, more-or-less with the IMF reversal regions. We also see that the opposite extreme, $\beta << 1$, occurs within the much larger region of the disturbed flow.

B2. Klein, L.W., and Burlaga, L.F. (1982) Interplanetary magnetic clouds at 1 AU, J. Geophys. Res. 87:613-624.

B3. Burlaga, L.F., Sittler, E., Mariani, F., and Schwenn, R. (1981) Magnetic loop behind an interplanetary shock: Voyager, Helios, and IMP 8 observations, J. Geophys. Res. 86:6673-6684.

B4. Wu, S.T., Han, S.M., and Dryer, M. (1979) Two-dimensional, time-dependent MHD description of interplanetary disturbances: simulation of high speed solar wind interactions, Planet. Space Sci. 27:255-264.

B5. Dryer, M., Wu, S.T., and Han, S.M. (1980) Two-dimensional, time-dependent MHD simulation of the disturbed solar wind due to representative flare-generated and coronal hole-generated disturbances, Geofis. Intern. 19:1-15.

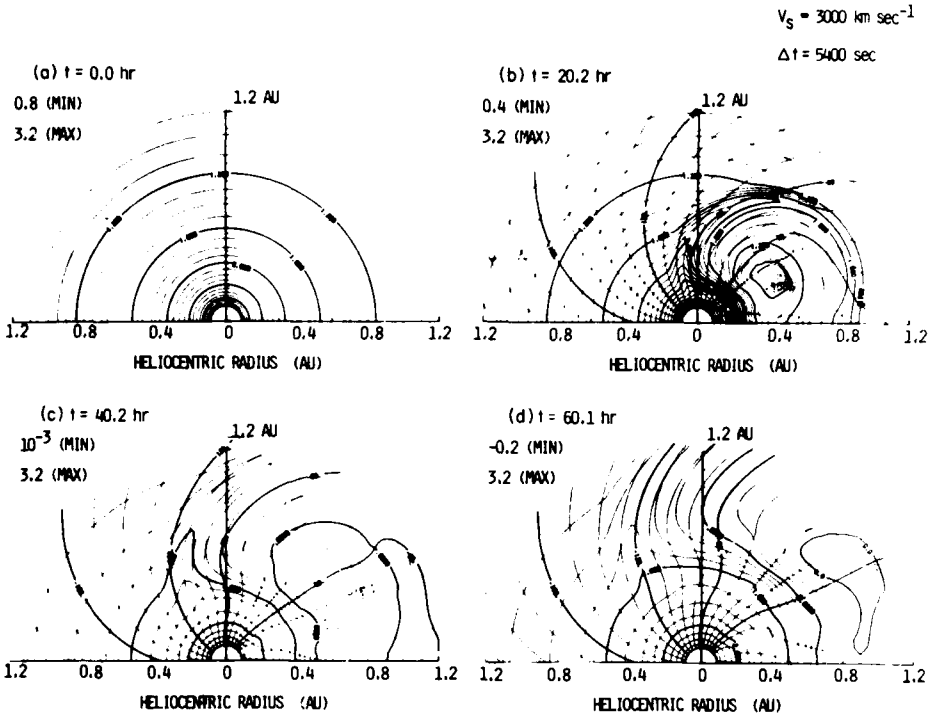

Figure B3. Density Contours, Together With Superposition of Deformed IMF (at t > 0 hr), Following Introduction of the Shock Wave, V_S = 3000 km sec^{-1}, Δt = 5400 sec. Numbers are Log_{10} (particles cm^{-3})

As discussed in several earlier papers (Dryer, Wu, and Han;[B5] Wu, Dryer, and Han[B6]), the results of n, T, P_{total}, and β appear to replicate the characteristics of magnetic clouds as observed and delineated by Klein and Burlaga.[B2] The characteristics to be discussed are shown for only one case: V_S = 3000 km sec^{-1} (Δt = 5400 sec), which is representative of the entire range of initial shock velocities mentioned earlier in the main text. It should be remarked that we made no special efforts to arrive at characteristics discussed by Klein and Burlaga, thus they were derived in a completely independent way. We, therefore, will continue to describe our results with comparative remarks, regarding the magnetic clouds, left for a discussion later in this appendix.

B6. Wu, S. T., Dryer, M., and Han, S. M. (1982) Non-planar MHD model for solar flare-generated disturbances in the heliospheric equatorial plane, submitted to Solar Physics.

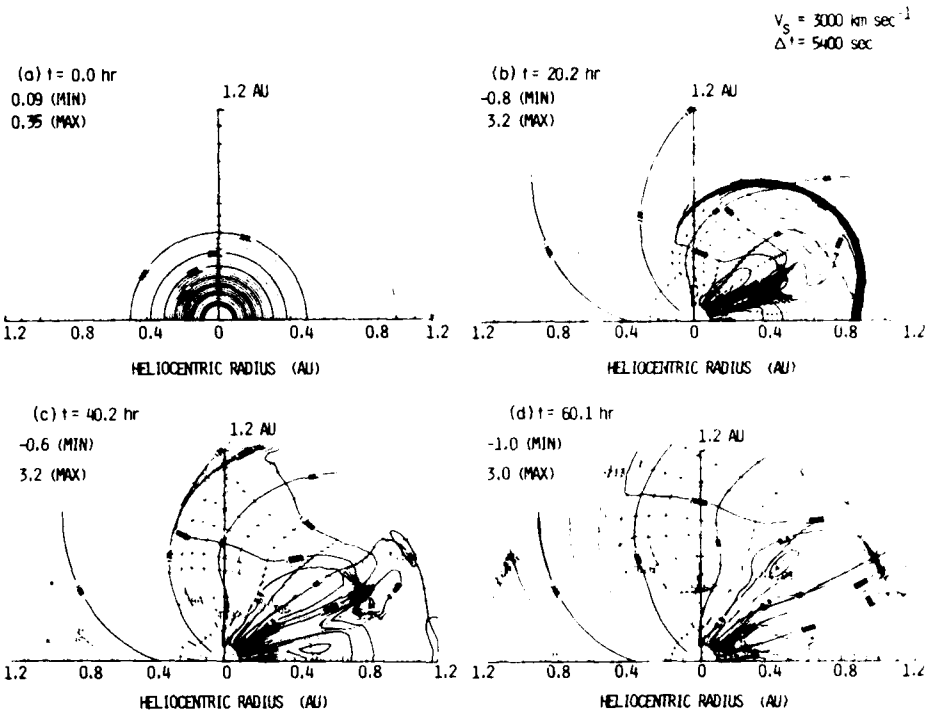

Figure B4. Plasma Beta ($\beta = 16\pi\, nkT/B^2$) Contours, Together With Superposition of Deformed IMF (at $t > 0$ hr), Following Introduction of the Shock Wave, $V_s = 3000$ km sec^{-1}, $\Delta t = 5400$ sec. Numbers are Log_{10}

Figure B5 shows the fractional temperature change, $(T - T_o)/T_o$, as the shock and post-shock flow pass through one quadrant of the computational domain. With reference to the half-tone scale given to the right side of Figure B5(a), we note that a very high Mach number shock (which is not unexpected since the initial velocity was so large) is seen at the flare's CM. The initial heating, of course, gradually decays as time progresses; eventually, an expanding region of cooler gas appears as seen at t = 80 hr in Figure B5(d). This result can also be seen in the contour plot of Figure B2(d) which shows, at t = 80 hr, temperatures as low as $10^{3.8}$ K, as compared with original values [Figure B2(a)] of $\sim 10^{4.6}$ ^{o}K at the same location close to the flare's CM.

Figure B6 shows the fractional density change, $(n - n_o)/n_o$, corresponding to the same times shown in the previous figure. Once again, as with Figures B2 and B3, we can compare the shock compression and heating, followed by adiabatic cooling and expansion in the sunward direction until the reverse shock is

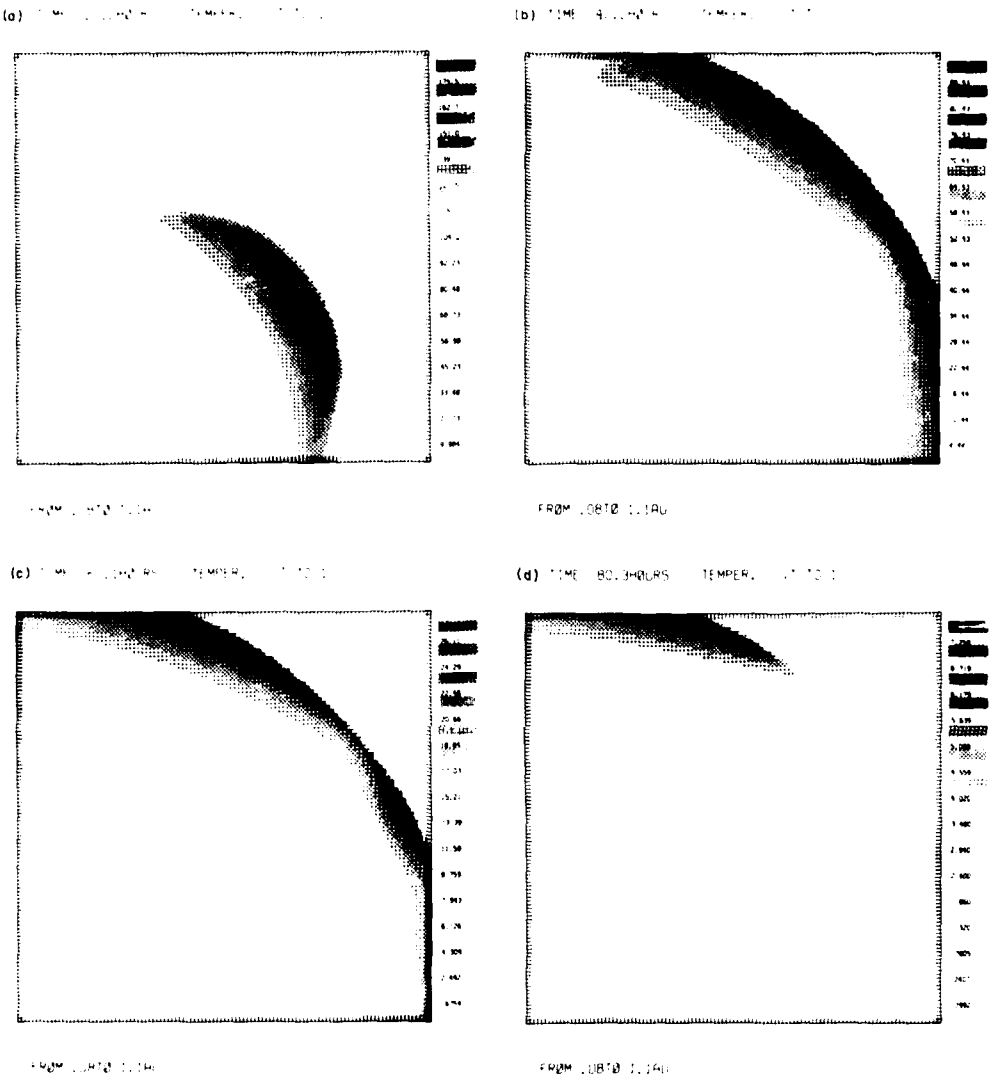

Figure B5. Fractional Temperature Change, $(T - T_o)/T_o$, Within Part ($0 \leq \phi \leq 90^o$) of the Calculational Domain. Note that the central portion of the fast forward shock has left the domain. Also, note the large region with no shading (see half-tone scale to the right of the lower right panel) with significant cooling relative to the ambient, undisturbed temperature: $(T - T_o)/T_o = -0.3$

encountered. The faster velocity, sunward of the reverse shock (Figure 3), flows through this discontinuity where a much lower level of heating and compression

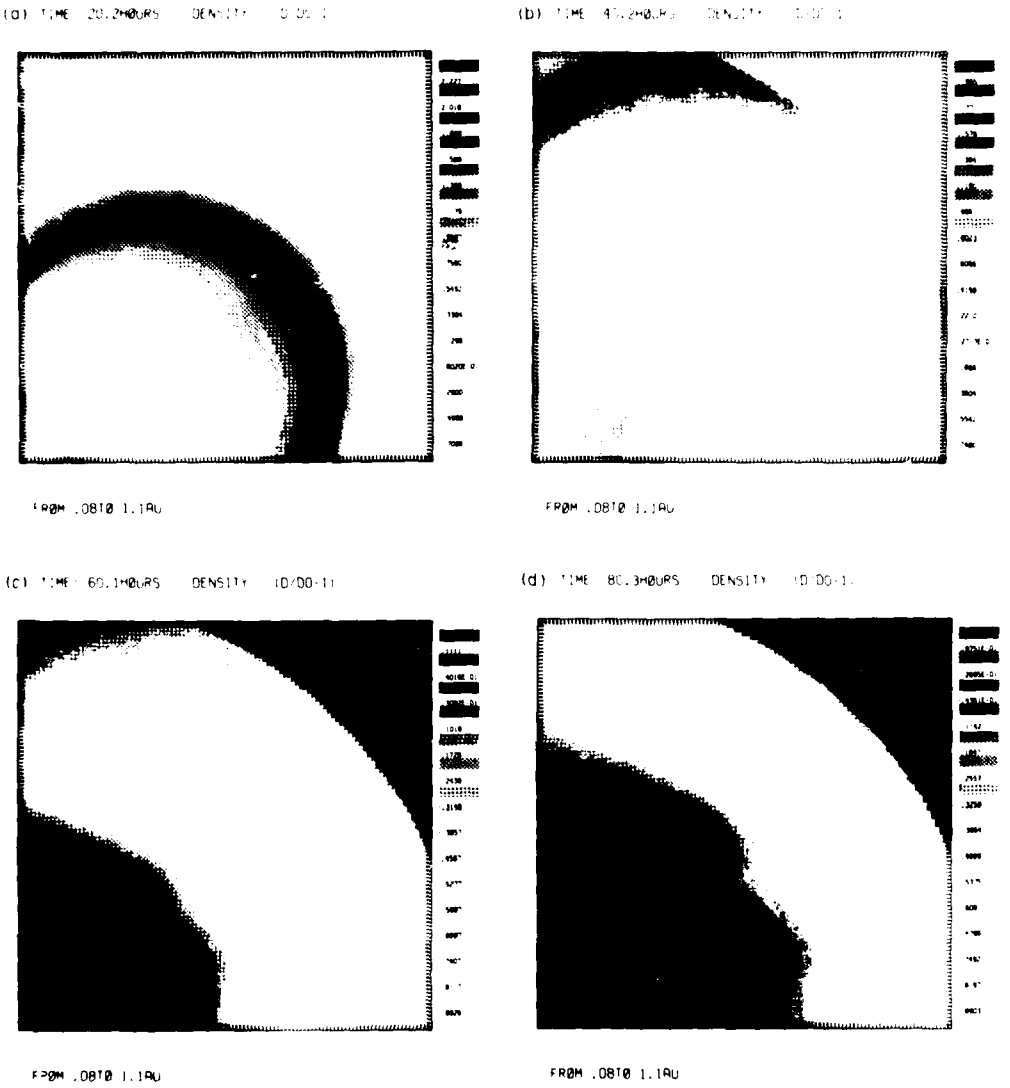

Figure B6. Fractional Density Change, $(n - n_o)/n_o$, Within Part ($0 \leq \phi \leq 90^o$) of the Computational Domain. Note that a substantial constantly-expanding region of depressed density levels follows within the two shocks' wake. Part of this region coincides with the depressed temperature region [compare Figure B6(d) with Figure B5(d)]

takes place. The overexpansion that follows behind the reverse shock (and its attenuated longitudinal extent) is apparent in each of the boxes in Figure B6 (as

noted by the negative values in the keyed half-tone scale next to each box). Note that the regions of depressed (lower than original steady-state values) temperatures and densities [Figures B5(d) and B6(d)] overlap in a scale size that, at 1 AU, is about 0.25 AU in longitudinal extent. Comparison of these two figures shows that the length-to-width ratio of the depressed density region is oriented in the ϕ-direction, whereas that of the depressed temperature region is oriented in the r-direction. We suspect that the region of overlapping, together with part of the region of IMF reversals, may constitute a magnetic cloud whose plane of minimum variance (of the IMF component perpendicular to it) is reasonably close to our equatorial plane. Klein and Burlaga[B2] noted that their set of 70 candidate magnetic cloud events included some ($\sim$ 25) for which the minimum variance direction was, indeed, nearly normal to the ecliptic plane.

Figure B7 shows the fractional change of total pressure, $(P_{total} - P_{total_o})/P_{total_o}$, where $P_{total} \equiv 2nkT + B^2/8\pi$. There is, of course, a rapid, precipitous increase as a result of the fast forward shock compression and heating. An observer at 1 AU along or near the CM would observe this rapid rise, followed by a gradual decrease over a period of about 3 days, as suggested by the results in Figures B7(a) - B7(c). Thereafter, for about 2 days, the total pressure would be predicted to decrease below its steady-state value. This result appears to contradict earlier discussions of cloud expansion due to high total pressure within them. In fact, it does. The earlier discussions implicitly assume that static equilibrium is present. By virtue of the time variance of *all* parameters at an observing spacecraft (see Klein and Burlaga[B2]), the flow is time variant in the spacecraft frame. Hence, a simplistic determination of a gradient of total pressure is insufficient to arrive at a valid conclusion concerning "cloud" expansion, cooling, etc. Here, we have assumed, implicitly, that reconnection need not take place; if true, extraneous bubbles might, in principle, float with the solar wind or even move relative to the plasma like a projectile. We think it premature at this time to require such exotic systems. Thus, we believe that a simple time-variant system as described here is sufficient for a fundamental, self-consistent understanding of the basic physical process for, at least, the shock-associated magnetic clouds described by Klein and Burlaga.[B2]

The discussion of temporal phenomena, as found by the MHD model, would be incomplete without a presentation of the plasma and field parameters at various observational points. In the paper by Wu, Dryer, and Han,[B6] we used the example of V_s = 1000 km sec^{-1} to present all parameters (including velocity and magnetic fields) at various points, each one considered separately. Here, we use a variation of this former presentation in order to emphasize heliolongitudinal attenuation of the basic physical quantities: radial velocity, density, temperature, and total magnetic field at 0.3 as well as at 1.0 AU.

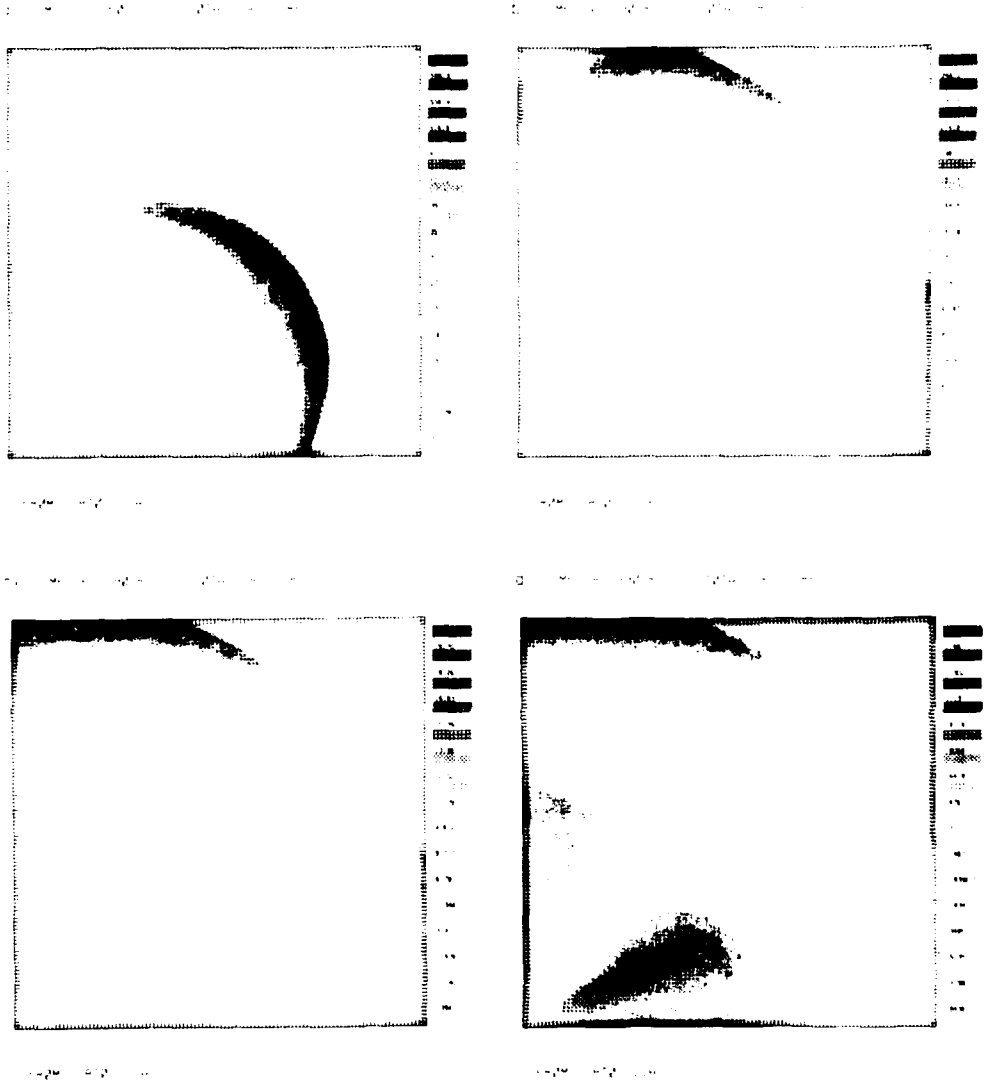

Figure B7. Fractional Total Pressure Change, $(P_T - PT_0)/PT_0$ Within Part ($0 < \phi < 90°$) of the Computational Domain. Note that the initially high values (relative to the undisturbed ones) gradually return after several days to the original state. Also note that P_T falls below the original state after 3 to 4 days within a narrowly-restricted radial zone as a result of the depressed temperatures and densities.

Figure B8 shows an array of these quantities at 0.7 AU as a function of time as they would be observed by a hypothetical spacecraft, such as Helios 1 and 2.

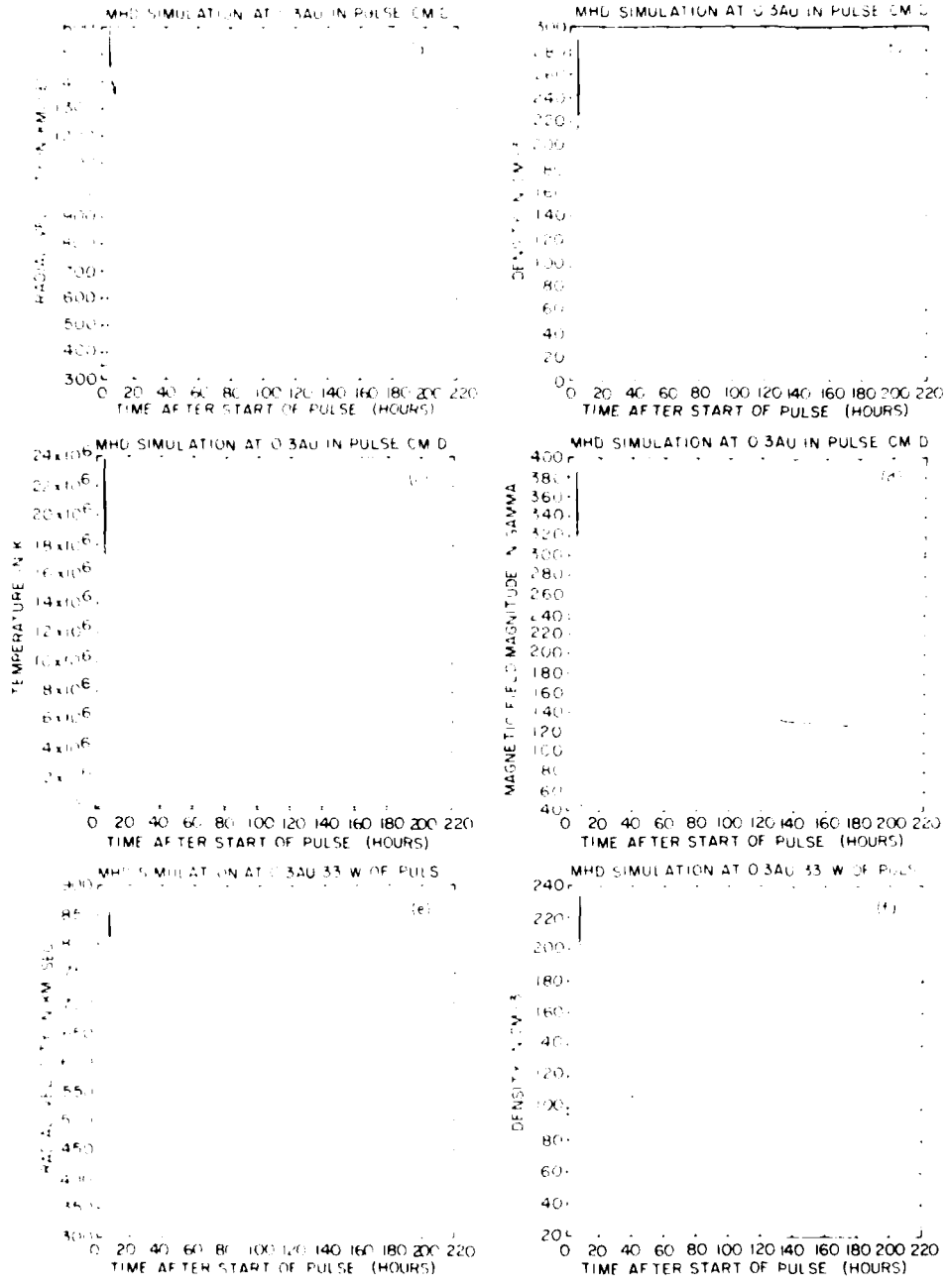

Figure B8. Time Series of Radial Solar Wind Velocity, Density, Temperature, and Total IMF Magnitude at 0.3 AU. (a) - (d) CM of flare-generated shock, (e) - (h) 33°W of CM, and (i) - (l) 90°W of CM

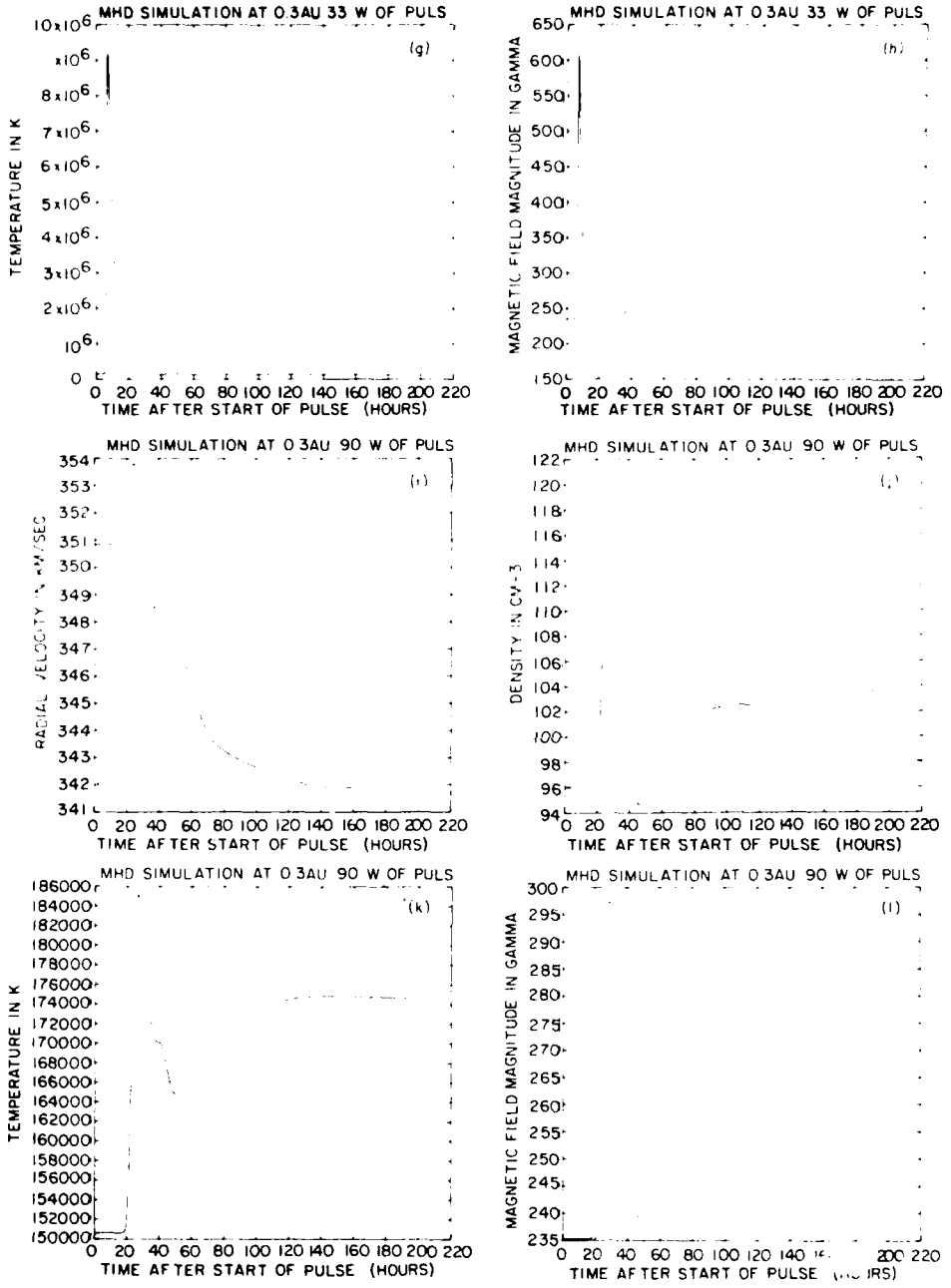

Figure B8. Time Series of Radial Solar Wind Velocity, Density, Temperature, and Total IMF Magnitude at 0.3 AU. (a) - (d) CM of flare-generated shock, (e) - (h) 33°W of CM, and (i) - (l) 90°W of CM (Contd)

(From a practical point-of-view, the two Helios spacecraft move very quickly through their 0.3 AU perihelia. Hence their hypothetical counterpart would "sample", only a short portion of the 200-hr series shown in Figure B7.) Figures B8(a) - B8(d) show the radial velocity, density, temperature, and total magnetic field at the CM of the canonical flare that produced a 3000 km sec^{-1} shock wave at $18R_s$, as used in the present simulation. The outstanding features are: (1) prompt arrival about 4 hr later of the fast forward shock followed at $t \simeq 10$ hr by the initiation and build-up of the fast reverse shock; (2) rapid compression, followed by an extensive rarefaction to greatly-reduced densities for about 50 hr before the recompression and very gradual return to the pre-disturbed values of density; (3) rapid heating to a temperature of $\sim 24 \times 10^6$ ^{o}K, which is common in a large flare; and (4) magnetic compression and rarefaction, accompanied by the strongly-deformed topology shown in Figure B1, with a recovery to only one-half its pre-disturbance value at the termination of the simulation. This is a real result and not a numerical artifact; the azimuthal and meridional IMF components return very nearly to their pre-disturbance values after the strong shock perturbation, but the radial component appears to respond in a wiggly fashion as the slow mode wave moves outward as well as in the longitudinal direction as discussed earlier in the discussion of Figures 3(e) - 3(g).

Panels (e - h) and panels (i - l) of Figure B8 show the same parameters at $33^{o}W$ and $90^{o}W$, respectively, of CM. Noting the increase of the vertical scale [especially for the case of $90^{o}W$ in Figures B8(i) - B8(l)], the delay (of arrival time) and attenuation of the peak velocity, density, and temperature at the forward shock (even at $90^{o}W$) are clearly seen. Note, however, that the peak IMF is increased at $33^{o}W$ (to 610 nT) relative to its peak value at CM (385 nT). The reason for this result is straightforward when one keeps in mind the fact that the shock propagates asymmetrically in a simultaneous radial and heliolongitudinal fashion. At CM, then, the shock is very nearly quasi-parallel - but not quite so; thus the IMF jump is [from Figure B8(d)] only from 235 nT to 385 nT. At $33^{o}W$, however, the shock normal inclination to the IMF ($\theta_{n,B}$) is larger than at CM; hence the magnitude jump [Figure B8(h)] is larger, from 235 nT to 610 nT despite some attenuation of the shock velocity in that direction. By $90^{o}W$, however, the shock velocity's attenuation overcomes the influence of a quasi-perpendicular value of $\theta_{n,B}$, and the jump [Figure B8(l)] is from 235 nT to only 297 nT.

Further, we explored a simple variation to our ansatz problem. What would be the Earth-oriented effect on ϵ and VB_θ if the B_θ component at $18R_s$ were initially an order of magnitude larger (10 nT) than the value, $B_{\theta_o} = 1$ nT, as used heretofore (Table 1)? To answer this question, we performed another calculation (about 3 min on the Cray-1, 33 min on the Cyber-750) with this change to the

parameters in Table 1. The results are shown in Figure B9. Contrary to a simplistic kinematic expectation, we did not obtain a larger ϵ simply as a result of an initially-larger southward IMF component. Figure B9(a) shows that the magnitudes of the two maxima are reduced below the 10^{19} erg sec^{-1} threshold that had otherwise been breached in Figure 6(a). On the other hand, VB_θ was increased by more than an order of magnitude, which would be in agreement with a kinematic interpretation that is not dependent upon a realistic evolution and kinking of the IMF.

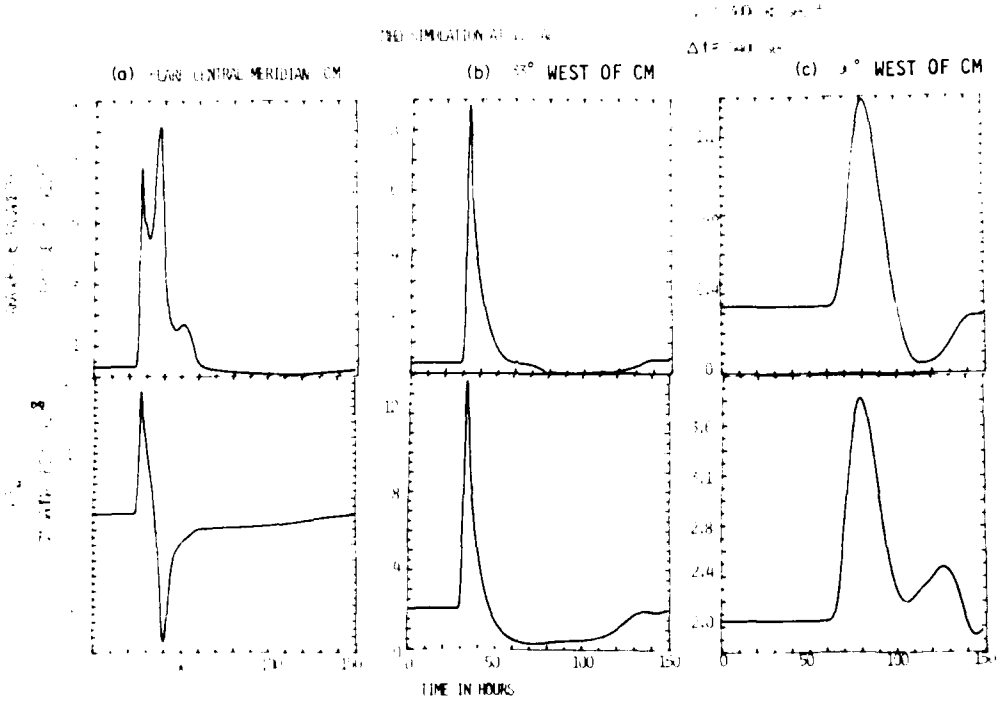

Figure B9. Energy Flux Parameter, ϵ, and the Product VB_θ at 1 AU For the Case: V_S = 3000 km sec^{-1}, Δt = 5400 sec, $B_{\theta O}$ = 10 nT (Instead of 1 nT, as Used Earlier). (a) CM, (b) 33°W of CM, and (c) 90°W of CM

This latter point concerning the evolution of the IMF brings us to our final comments regarding the earlier "magnetic cloud" discussion. We cross-plotted the IMF components against each other (without performing a minimum variance computation in this early exploratory work) for the case V_S = 3000 km sec^{-1}.

Δt = 5400 sec; B_{θ_o} = 10 nT. The results are shown in Figure B10 in the form of polar plots assuming that the equatorial plane is a reasonable approximation to the true plane of minimum variance. It can be seen that, indeed, the excursion of B_θ does not exceed ± 20 nT, whereas the B_ϕ component has an excursion to nearly 80 nT in the eastward direction. It is of interest to note that a rotation of nearly 90° of the IMF field, projected into the equatorial plane, takes place. (It is also seen in Figure B1(c), at positions east of CM for the previous case, that a 180° rotation takes place.)

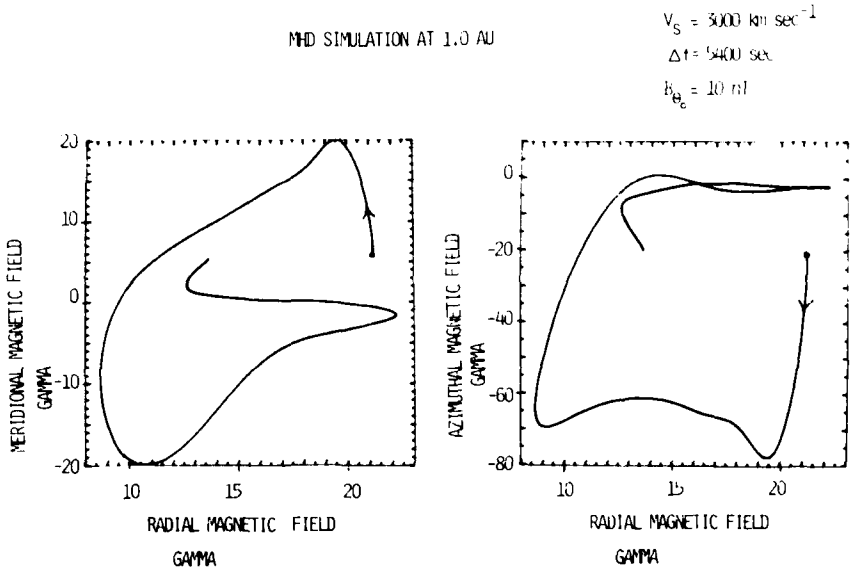

Figure B10. Polar Plots of IMF at 1 AU, CM, For the Case: V_S = 3000 km sec^{-1}, Δt = 5400 sec, B_{θ_o} = 10 nT. Note the scale change between B_ϕ and B_θ

References

B1. D'Uston, C., Dryer, M., Han, S. M., and Wu, S. T. (1981) Spatial structure of flare-associated perturbations in the solar wind simulated by a two-dimensional numerical MHD model, J. Geophys. Res. 86:525-534.

B2. Klein, L. W., and Burlaga, L. F. (1982) Interplanetary magnetic clouds at 1 AU, J. Geophys. Res. 87:613-624.

B3. Burlaga, L. F., Sittler, E., Mariani, F., and Schwenn, R. (1981) Magnetic loop behind an interplanetary shock: Voyager, Helios, and IMP 8 observations, J. Geophys. Res. 86:6673-6684.

B4. Wu, S. T., Han, S. M., and Dryer, M. (1979) Two-dimensional, time-dependent MHD description of interplanetary disturbances: simulation of high speed solar wind interactions, Planet. Space Sci. 27:255-264.

B5. Dryer, M., Wu, S. T., and Han, S. M. (1980) Two-dimensional, time-dependent MHD simulation of the disturbed solar wind due to representative flare-generated and coronal hole-generated disturbances, Geofis. Intern. 19:1-15.

B6. Wu, S. T., Dryer, M., and Han, S. M. (1982) Non-planar MHD model for solar flare-generated disturbances in the heliospheric equatorial plane, submitted to Solar Physics.